Chapter 7
Supramolecular Liquid Crystals Based on Cyclodextrins

Pier-Luc Champagne, Rajesh Kumar, and Chang-Chun Ling

Contents

Abstract Cyclodextrin-based materials represent an environmentally friendly alternative to toxic liquid crystalline materials. Cyclodextrins are well-known for their cavity and inclusion properties. They are scaffold molecules that can be chemically modified to obtain functional materials for various applications. For instance, amphiphilic cyclodextrins have attracted tremendous interests from researchers of different fields because of their ability to self-assemble and to encapsulate medicines. They can also be designed to form supramolecular liquid crystals. Since the first report of a class of 6-alkylthiolated β-cyclodextrin derivatives that exhibit ther-

P.-L. Champagne · R. Kumar · C.-C. Ling (✉)
Alberta Glycomics Centre, Department of Chemistry, University of Calgary, Calgary, Alberta, Canada
e-mail: ccling@ucalgary.ca

S. Fourmentin et al. (eds.), *Cyclodextrin Applications in Medicine, Food, Environment and Liquid Crystals*, Environmental Chemistry for a Sustainable World, https://doi.org/10.1007/978-3-319-76162-6_7

motropic liquid crystalline properties in 1993, there has been only few developments in this area. But there is an increasing interest to develop cyclodextrin-based liquid crystalline materials, owing to their potential utilities in different areas.

In this chapter, we review cyclodextrins-based molecular designs, their synthesis, as well as characterization of their thermotropic and lyotropic liquid crystalline properties. The presence of numerous hydroxyl groups and a face-to-face pseudo-symmetry in native cyclodextrins create numerous opportunities for the design of smart materials. It has been shown that not only the nature of the substituent, but also its location highly influences the self-assembly behavior of the cyclodextrin derivatives. After an introduction on cyclodextrins and liquid crystals, we summarize various approaches used to chemically modify cyclodextrins for the development of thermotropic and lyotropic liquid crystals, such as generating amphiphilic derivatives, or appending mesogenic groups to both monomeric and polymeric cyclodextrin backbones. The last section presents examples of applications of cyclodexrin-based liquid crystals for bio-sensing and liquid crystal displays.

7.1 Introduction

7.1.1 Cyclodextrins Structures

Cyclodextrins (CDs) are polyhydroxylated macrocycles based on D-glucose. The three most commonly encountered members are α-, β- and γ-CDs which contain 6, 7 and 8 D-glucopyranosyl units, respectively giving birth to a characteristic truncated cone-shaped cavity of different sizes (Fig. 7.1).

The inner cavity volume of these cyclodextrins vary between 0.17–0.42 nm^3 and their diameters from 0.49 to 0.79 nm. The cavities of cyclodextrins are relatively hydrophobic compared to outer surface, which provides them with ability to form inclusion complexes with organic guest molecules that are characterized with improved water-solubility, air-stability, reduced tissue-irritability, and other benefits. The electrochemical potential map of β-cyclodextrin shown in Fig. 7.2**,** greatly

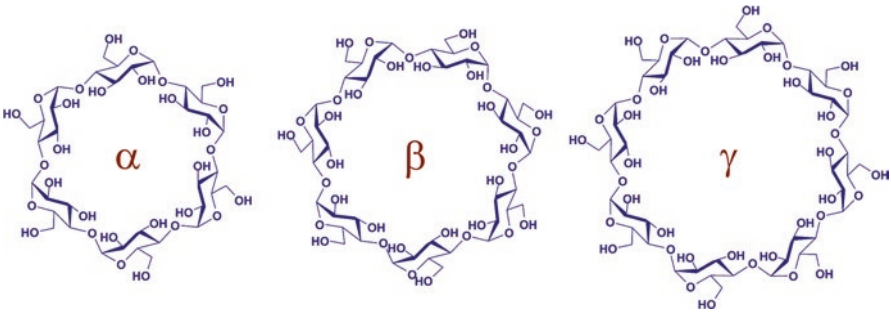

Fig. 7.1 Graphical representation of the three most commonly encountered cyclodextrins; α, β, and γ cyclodextrins

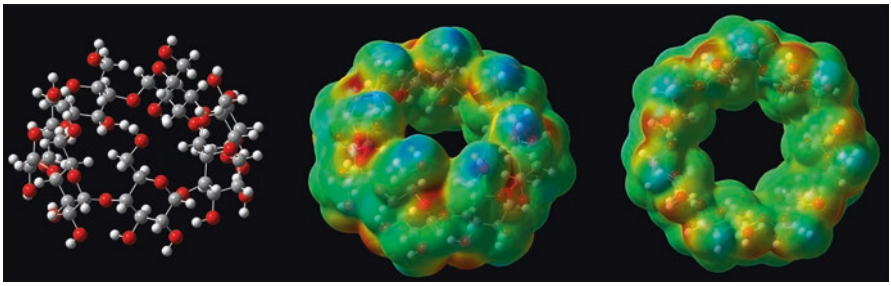

Fig. 7.2 Electrochemical potential map of the truncated cone-shaped structure of β- cyclodextrin

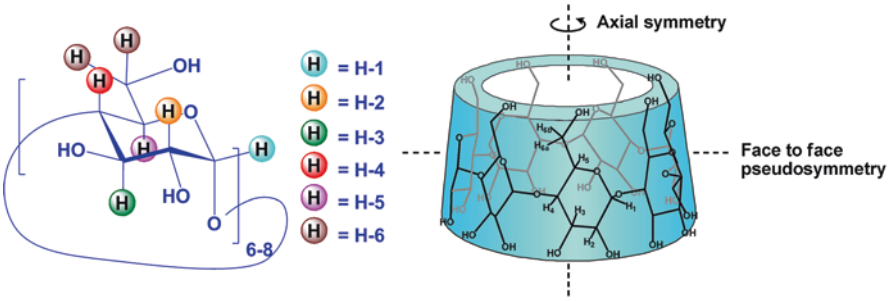

Fig. 7.3 Commonly used nomenclature for hydrogens in native cyclodextrins as well as their axial symmetry and face to face pseudosymmetries

represents the hydrophobic character of cyclodextrins cavity. The red, blue and green colors illustrate the negative, positive, and neutral electrochemical regions, respectively. Such representation emphasizes the contrast between the hydrophobic inner cavity and hydrophilic outer-surface of cyclodextrins.

For these reasons, cyclodextrins have attracted considerable attention from pharmaceutical and other industries (Hirayama and Uekama 1999; Rasheed 2008). Structurally, the D-glucose units are linked together via α(1,4)-glycosidic linkages, which arranges all the primary hydroxyl groups (OH-6's) at the narrower face (primary face) of the cavity, and all the secondary hydroxyl groups (OH-2's and OH-3's) at the wider face (secondary face) (Fig. 7.3).

Consequently, all cyclodextrins possess an axial symmetry, as well as a face-to-face pseudo symmetry. Although cyclodextrins improve aqueous solubility of hydrophobic molecules, they are unfortunately restrained by their own solubility in aqueous media. α, β, and γ- cyclodextrins have a water solubility of 14.5%, 1.85%, and 23.2% (w/v) respectively at room temperature (Davis and Brewster 2004). Their lower solubility is partly attributed to the intramolecular hydrogen bond network which lessens their ability to form H-bonding with water molecules (Rasheed 2008). Enhanced solubility can be achieved by reducing the strength of this network. For instance, partial methylations of cyclodextrins have shown to increase water-solubility tremendously (Rasheed 2008). Because of their high polarity,

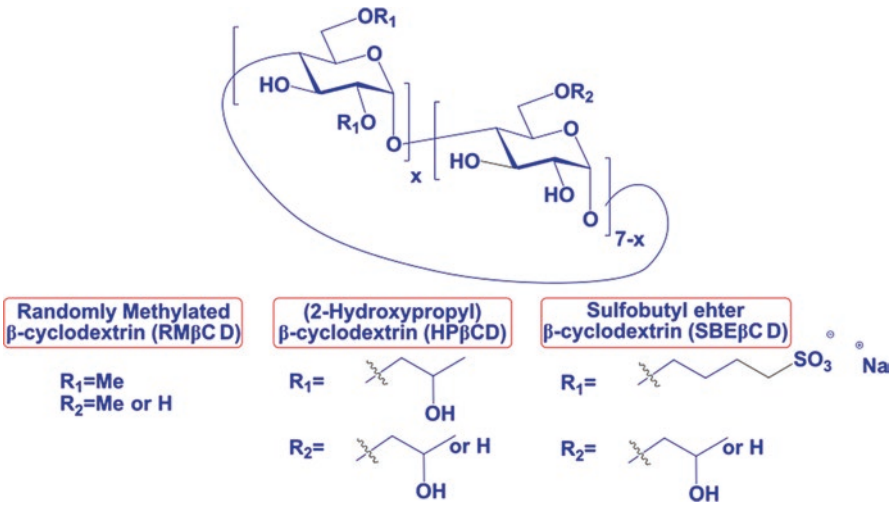

Fig. 7.4 Structures of commercially available CD derivatives; randomly methyl-β-cyclodextrin (RMβ-CD), 2-hydroxypropyl β-CD (HPβCD), and sulfobutyl ether (SBEβ-CD)

native cyclodextrins also have very limited solubility in most organic solvents. To expand their applications in pharmaceutical industries, various chemical modifications have been developed. The three most widely used and commercially viable strategies are to partially alkylate the β-cyclodextrin scaffold with methyl, 2-hydroxypropyl, or sulfobutyl groups, to afford respectively RMβ-CD, HPβ-CD and SBEβ-CD (Fig. 7.4). Unfortunately, due to coexistence of multiple types of hydroxyl groups and limited differences in their reactivity, all chemically modified cyclodextrin derivatives available on the market are sold as mixtures that contain different degrees of substitutions (Rasheed 2008).

7.1.2 Cyclodextrin Modifications

At first sight, since the hydroxyl groups are the only available functional group present at the two rims of the cavity, one might believe cyclodextrin chemical modifications to be simple but they are in fact very challenging, due to their presence in large number. Three types of hydroxyl groups can be identified within a native cyclodextrin molecule: those respectively attached to 2, 3, and 6-positions of glucopyranosyl units (Szejtli and Huber 2012). In the case of β-cyclodextrin, each type of hydroxyl groups consists of 7 identical copies. Due to the circular geometry, the hydroxyl groups of the seven glucose moieties form an intramolecular H-bonding network, resulting in a relatively rigid structure. At the primary face, the primary hydroxyl groups attached to the 6 positions have an additional degree of rotational freedom, making the hydrogen bond network weaker. More importantly, they experience lower

steric hindrance, resulting in higher reactivity (Khan et al. 1998). On the other hand, all secondary hydroxyl groups located at the 2- and 3-positions experience reduced rotational freedom allowing the formation of a stronger hydrogen bond network. Furthermore, the increase in steric hindrance contributes to their lower reactivity.

X-ray experiments revealed that the OH-3 groups act as H-bond donors while the OH-2 as H-bond acceptors; this makes OH-2's the most acidic (Saenger et al. 1976). Since the protons of OH-3 groups are involved in intramolecular hydrogen bonding, they are generally less reactive, thus most challenging to modify. Consequently, by controlling the reactivity of the chemical reagent used, one can achieve regioselective modification of cyclodextrins. For instance, the OH-6's can be selectively protected with bulky groups such as *tert*-butyldimethylsilyl, while less bulky group such as trimethysilyl can be introduced to all 3 positions (Cramer et al. 1969; Takeo et al. 1988). The most acidic OH-2 groups can be deprotonated first to allow selective OH-2 monoalkylation. However, the proton exchange between the OH-2 and OH-6 positions often reduces the regioselectivity which produces mixtures of O2- and O6-substituted derivatives (Khan et al. 1998).

Since cyclodextrins possess the capability to form complexes, it is possible in few cases to achieve regioselective modifications by taking advantage of their inclusion properties (Ueno and Breslow 1982). This process is greatly influenced by the solvent effect and the size of the substituted cyclodextrin cavity. For instance, the 6-tosylated-α-cyclodextrin product is obtained in pyridine, while the reaction in aqueous media yields the mono-2-tosylate α-cyclodextrin. On the other hand, if β-cyclodextrin is subjected to a monotosylation in water, the 6-tosylate is obtained (Fujita et al. 1984).

In general, since the OH-6's in cyclodextrins are the most nucleophilic and least sterically hindered, per-substitutions at the primary face are less troublesome. On the other hand, since all primary hydroxyl groups have identical chemical reactivities, partial substitutions such as mono-, di-, and tri-substitutions are usually much more challenging, as they usually lead to the formation of many regioisomers (also referred to as positional isomers) which are extremely difficult to separate. Consequently, partial substitutions usually result in low yields of the desired product.

Persubsitutions at the secondary face are especially difficult because of the inherited lower chemical reactivity of secondary hydroxyl groups. Moreover, there are twice the amounts of –OH groups at the secondary face compared to primary face; as the reaction progresses, the reactive sites become increasingly more hindered, making the approach of electrophiles more challenging.

7.1.3 Synthesis of Amphiphilic Cyclodextrins

The face-to-face pseudosymmetry (Zhang et al. 1992) can be taken advantage of by chemical modifications, to introduce hydrophobic groups to only one face of the molecule. This results in the formation of amphiphilic molecules. These amphiphilic cyclodextrins act like detergent in water, thus possess the ability to form

self-assembled systems (Bonini et al. 2006). Depending on the size and geometry of the introduced hydrophobic groups, different nano-materials can be obtained through their self-assembly (Nagarajan 2002) such as spherical micelles, liposomes and other rod-like objects (Nagarajan 2002). Once assembled into such self-organized structures, the inherent cyclodextrin cavity and the hydrophobic regions found within the apolar chains can be used to host the hydrophobic guest molecules, creating efficient drug delivery systems for the treatment of disease. This has attracted considerable interest from pharmaceutical researchers (Rajewski and Stella 1996; Challa et al. 2005; Hoare and Kohane 2008). Such amphiphilic systems are advantageous compared to non-amphiphilic cyclodextrins which can only encapsulate the desired cargo into the hydrophobic cyclodextrin cavity, for enhanced distribution of drug to the disease model. By forming self-assembled nanostructures, a concentrating effect may be achieved, with many replicas of the drug trapped in one nanostructure. Upon administration, self-assembled nanoparticles can reach the targeted disease cells, and deliver replicas of drug molecules at the same time, thus augmenting the therapeutic potency and efficacy (Yallapu et al. 2010). Consequently, this could greatly improve drug safety while reducing toxicity, as lower dosage could be administered without diminishing the overall therapeutic effect of the medicine (Rajewski and Stella 1996).

Amphiphilic cyclodextrin complexes can be designed to control the average release rate of a drug. In fact, cyclodextrins have been modified to offer a desired drug-releasing mechanism to improve the oral bioavailability of steroids, cardiac glycosides, non-steroidal anti-inflammatory drugs, benzodiazepines etc. (Rasheed 2008). For instance, when a drug has to be delivered to the enteric region, a delayed release is required to prevent premature leaking of the cargo into the stomach, which presents a harsh acidic environment. In order to reach the upper small intestine, a cyclodextrin-based drug delivery system (DDS) bearing weak acidic groups at its surface was designed. Such formulations display reduced solubility in the stomach while increased solubility in neutral and alkaline regions, owing to ionization of the acidic groups. This pH dependent behavior allows a delayed release of the drug into the enteric region. As an example, 6-*O*-(carboxymethyl)-β-cyclodextrin derivatives have been developed as a drug delivery system for time-controlled release of oral medicine; the system exhibited restricted solubility in acidic conditions but improved solubility with increasing pH (Uekama 2004).

7.1.4 Liquid Crystals

Self-assembly of simple systems into well-ordered nano-structures is a fascinating topic. The understanding of the fundamentals of soft-matter self-organization has stimulated tremendous research interest throughout the last decade (Hoeben et al. 2005; Yagai and Kitamura 2008). Liquid crystal represents a state of the matter between solid and liquid phase. It displays the fluidity of liquids while possessing the molecular alignment of crystalline solid. Liquid crystalline phases are referred

to as mesophases and the molecules responsible for such behavior, as mesogens. In order to obtain spontaneous self-assembly of specific material into highly-ordered molecular structures at nanoscales, molecular building blocks must be precisely engineered to display the desired characteristics. In an attempt to improve our understanding of such phenomena, some background information about the transitions from crystalline solid to isotropic liquid will be discussed.

Commonly, two main parameters are used to report molecular arrangement in different phases, the orientational order which describes the alignment of molecules to a director (n), and the positional order which refers to the center of mass of each molecule with respect to each other. A material in crystalline solid phase is composed of molecules having both positional and orientational order with periodically repeating patterns. Such nanoscale organization is possible because of non-covalent intermolecular forces. Within the crystalline phase, the sole movement of the molecules is the thermal vibration within the crystal lattice (Gray 1962). As the temperature increases, these vibrations become stronger and eventually overcome the intermolecular interactions. At the transition temperature (melting), the solid material enters an isotropic liquid phase. It can be rationalized that at such temperature, the long range positional order is destroyed, providing freedom to the molecules for random traveling.

On the other hand, some materials possess liquid crystalline phases, associated with transitions observed between the crystalline and isotropic liquid phases, characterized by the presence of either positional or orientational order or both. Higher degrees of orientational order give the mesophase enhanced anisotropic properties while lower degrees of positional order provide greater fluidity (McArdle 1990).

Liquid crystals are classified into two main families: thermotropic and lyotropic. Thermotropic liquid crystals are formed from pure products which self-organize into mesophases upon temperature variation. In contrast, lyotropic liquid crystals are formed by the addition of solvent to an amphiphilic molecule, resulting in long range positional orders due to the self-organization properties of the molecule.

Throughout this chapter several examples of cyclodextrin-based liquid crystal designs will be discussed. First, cyclodextrin-based thermotropic liquid crystals will be presented and rationalized based on the interactions and substituents responsible for their self-assembly. In the second section, lyotropic liquid crystalline systems containing cyclodextrins will be discussed, as well as some of their potential applications.

7.1.5 Thermotropic Liquid Crystals

Thermotropic liquid crystals are materials whose self-assembly behavior is influenced by temperature variation in the solid states. They can exist in many different phases. The three most common phases are: nematic (Fig. 7.5), smectic (Fig. 7.6) and discotic (Fig. 7.7) liquid crystalline phases.

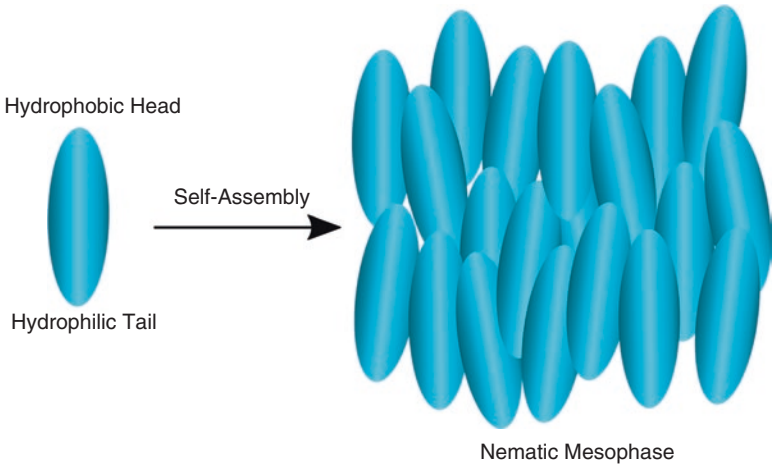

Fig. 7.5 Pictogram representation of molecular arrangement in the nematic liquid crystalline mesophases

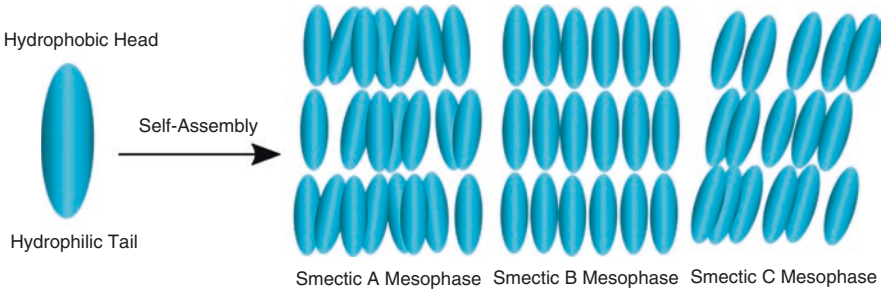

Fig. 7.6 Pictogram representations of molecular arrangement in the smectic A, B, and C liquid crystalline mesophases

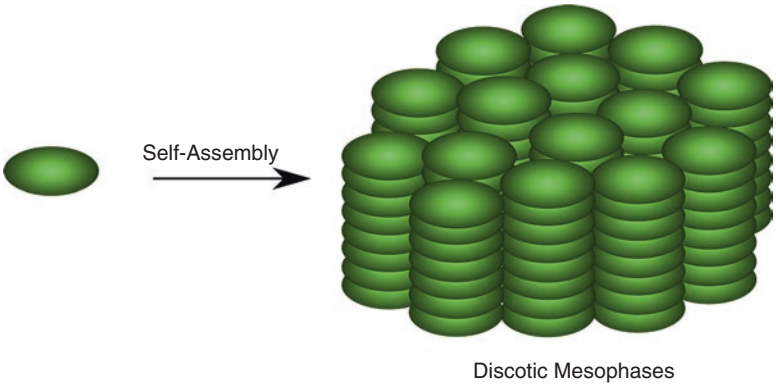

Fig. 7.7 Pictogram representations of molecular arrangement in the discotic liquid crystalline mesophases

7.1.5.1 Nematic Phase

The nematic phase (N) is the thermotropic liquid crystalline phase with the least order. This phase is characterized by self-organization of molecules into ordered structures in which the long axis of all molecules (director **n**) aligns with each other, procuring orientational order to the material. However, no positional order is found in nematic liquid crystalline phase since the center of mass of the molecules is isotropically distributed (Linlin et al. 2015).

7.1.5.2 Smectic Phases

Smectic mesophases are often observed when decreasing the temperature of nematic phase. They possess some degree of positional order in addition to the orientational order. The center of mass of the molecules aligns more or less with each other, forming layered structures (Collings and Hird 1997). Within the same layer, the molecules can move around, gain some degree of freedom but overall all molecules maintain a degree of translational order. Several types of smectic phases are known depending on the type and degree of order (Fig. 7.6). The least ordered smectic mesophase is called Smectic A (Sm A). Sm A mesophases consist of layered structures in which the director **n** is parallel to the layer normal but possess no order within the layers. Other smectic mesophases, such as Smectic C, differ from Smectic A by the tilted angle of their director **n**, with respect to the layer normal. Several other smectic mesophases are also known such as Smectic B, I, and F, which are generally characterized by the intra-layer short range positional order. They are also referred to as hexatic smectic phases. Within these phases, the center of mass of the molecules arranges in hexagonal pattern. The three different hexatic smectic phases (Sm B, Sm I, Sm F) differ in their respective director **n** orientation. Sm B director **n** aligns parallel to the layer normal, while in the case of Sm I, **n** is tilted towards the corner of the hexagon (apex), contrasting with Sm F whose director **n** is tilted towards the side of the hexagon.

7.1.5.3 Discotic Liquid Crystal

Discotic mesophases are usually formed by disk-shaped molecules which orient themselves in a layer-like fashion and packed into stacks (called discotic columns, Fig. 7.7). Similarly to smectic mesophases, the columns formed can possess random or ordered positions by arranging themselves into cubic or hexagonal arrays (Kumar 2010).

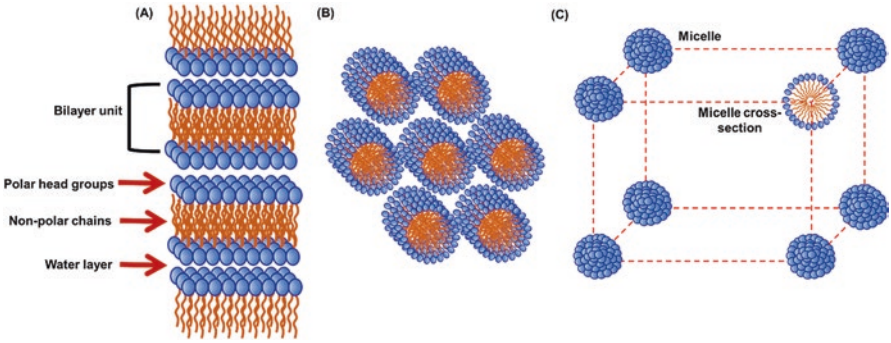

Fig. 7.8 Various types of lyotropic liquid crystals; (**A**) Lamellar, (**B**) Hexagonal, and (**C**) Cubic

7.1.6 Lyotropic Liquid Crystals

Lyotropic liquid crystals, consist of two-component systems mostly displayed by amphiphilic molecules in solvent producing ordered mesophases (Hiltrop 1994). Lyotropic liquid crystals morphologies are highly dependent on concentration and temperature of the amphiphilic systems bearing hydrophilic head and hydrophobic tail (Tolédano and Neto 1998). At critical micelle concentration (CMC) in aqueous solutions, amphiphilic molecules aggregate into micelles with polar head groups directed outward and hydrophobic tails inward. Upon increasing the concentrations, the micelles can fuse to each other forming various types of lyotropic liquid crystals such as cubic micelles, hexagonal phase, cubic phase and lamellar bilayer phases. The lamellar phase consists of amphiphilic molecules arranged in bilayer structures (Fig. 7.8A). The non-polar tails of two oppositely directed molecules are intertwined into the inner membrane and polar head groups found at the surface. The bilayer structures resulting from this self-assembly are separated by layers of water at the interface. Generally, lamellar lyotropic liquid crystal phases are obtained in solution of amphiphilic molecules concentrations higher than 50%.

In hexagonal phase, micelles are fused together; forming long ranged hexagonal cylinder arrays that exhibit birefringent textures (Fig. 7.8B). The distance between adjacent micellar cylinders is approximately 1 to 5 nm depending upon the concentration of amphiphilic and solvent molecules. Typically, hexagonal lyotropic liquid crystals are highly viscous with water content of 30 to 60% by weight. Cubic lyotropic liquid crystal phase, on the other hand, shows cubical arrangements of micelles that lead to viscous isotropic phases (Fig. 7.1C).

7.2 Cyclodextrin-Based Thermotropic Liquid Crystals

In the following section, several cyclodextrin-based thermotropic liquid crystals will be discussed. Based on their designs, they can be classified into three families: (a) cyclodextrin liquid crystalline systems that combine simple aliphatic chains and polar groups; (b) cyclodextrin liquid crystals that have incorporated mesogenic groups; (c) polymer-based cyclodextrin liquid crystals.

7.2.1 Thermotropic Liquid Crystals Based on Simple Amphiphilic Cyclodextrin Derivatives

7.2.1.1 H-Bond Mediated Mesophase Formation Based on Amphiphilic Cyclodextrin Derivatives

The early generations of amphiphilic cyclodextrin derivatives were prepared by introducing hydrophobic alkyl groups such as alkylamino, alkylthio, or alkylsulfonyl to the primary face of β-cyclodextrin. (Tanaka et al. 1987; Taneva et al. 1989). Unfortunately, these derivatives were a commonly prepared via the "per-6-tosylate of β-CD" through S_N2 substitutions. It was later found that the "per-6-tosylate of β-cyclodextrin" could only be isolated in pure form and in low yields by repeated high-performance liquid chromatography using reversed phase C18 column. This confirmed that the amphiphilic cyclodextrins prepared earlier were impure as they contained mixtures with different degrees of substitutions. (Ashton et al. 1991) Despite the heterogeneity in these materials, they were found to possess excellent properties in self-assembly such as forming mono-layer and Langmuir-Blodgett films at the water-air interface, micelles and liposomes in water etc. However, their thermotropic properties remained unknown until 1993 when Ling and Darcy (Ling et al. 1993) published the first series of cyclodextrin-amphiphiles that showed thermotropic liquid crystalline properties. Their successful synthesis began with the use of per-6-bromo-6-deoxy-β-cyclodextrin, which was prepared from native β-cyclodextrin **1** using Gadelle and Defaye's protocol (Gadelle et al. 1991) which employs Br_2/Ph_3P as a reagent in anhydrous dimethylformamide. This afforded the per-6-deoxy-6-bromo-β-cyclodextrin **2** in excellent regioselectivity and high purity. The subsequent per-substitution by alkylthiolate of different lengths allowed them to synthesize per-6-alkylthio-substituted amphiphilic β-cyclodextrin derivatives **3a-e** in excellent yields (>90%) and purities (Fig. 7.9).

The incorporated chain lengths varied from C_2-C_{18}, which provided them opportunities to comprehensively study the thermotropic properties of this family of amphiphilic cyclodextrins. Both cross-polarized optical microscopy (POM) and differential scanning calorimetry (DSC) were used to determine the phase transitions of the materials upon heating and cooling, and cross-polarized optical microscopy further provided information on the birefringence of the material during phase tran-

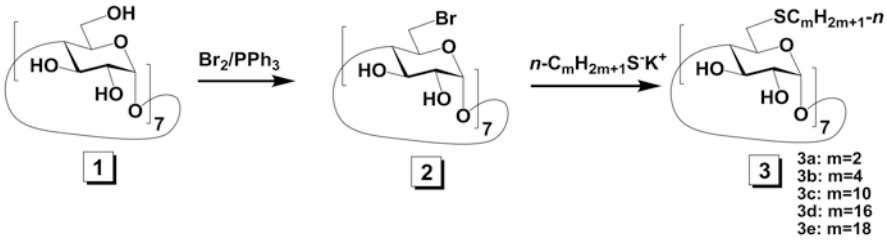

Fig. 7.9 Synthetic scheme of the first family of amphiphilic cyclodextrins that displayed mesogenic properties

sitions and formed textures. It was discovered that although all synthesized compounds showed some degrees of thermotropic liquid crystallinity, compounds **3d** and **3e** that contain chain lengths of 16 and 18 carbons respectively, displayed the best mesogenic properties over a wide temperature range (215 to 280 °C). However, upon heating further, both compounds decomposed before reaching their isotropic liquid phase. By comparing the textures of the two cyclodextrin compounds to monosaccharide mesogens bearing a single chain, the authors assigned the formed mesophases by compounds **3d** and **3e** to be smectic; thus, bilayer structures were proposed in the formed liquid crystalline phases. When analyzed by X-ray powder diffraction, derivative **3e** revealed a sharp peak in the low angle region which was attributed to a bilayer depth of 38 Å, less than twice the calculated molecular length. The authors suggested that the CD molecules may exist at some degrees of inclination in the layers. In the later work, Ling and co-workers (Ward et al. 2014) explained the results using an interdigitation model by the amphiphilic CD molecules in the bilayer (Fig. 7.10).

H-bonding was believed to be the major intermolecular force that drives the amphiphilic cyclodextrin molecules to self-assemble into highly ordered liquid crystalline mesophases. Because of their cyclic bidimensional geometry, amphiphilic cyclodextrin molecules can establish complex inter- and intra-molecular H-bond network in solid state. To elucidate the important role that H-bond played during the molecular self-assembling, Ling and co-workers (Ward et al. 2014) prepared a series of per-6-substituted β-cyclodextrin derivatives (**4**–**9**), all modified with the *n*-octadecylthio group at the 6-positions (Fig. 7.11).

Compounds **4** and **5** were per-substituted at all O2 and O3 positions with methyl and benzyl groups respectively, thus they contained no hydroxyl groups, therefore were incapable of inducing molecular self-assembly via H-bonding in solid state. However, in principle, molecules of compound **5** could interact with each other via π-π interaction in solid state because of their phenyl groups. Compounds **6**–**9** are all amphiphilic as they were regioselectively modified at all O2 positions with alkyl groups, namely methyl **6**, ethyl **7**, allyl **8** or benzyl **9**, but all possess seven hydroxyl groups (OH-3's). Thus, all compounds **6**–**9** should be capable of intermolecular H-bonding in solid state. On the other hand, since the alkyl groups at O2 position increase in size from **6** to **9**, their physical dimensions could effectively determine

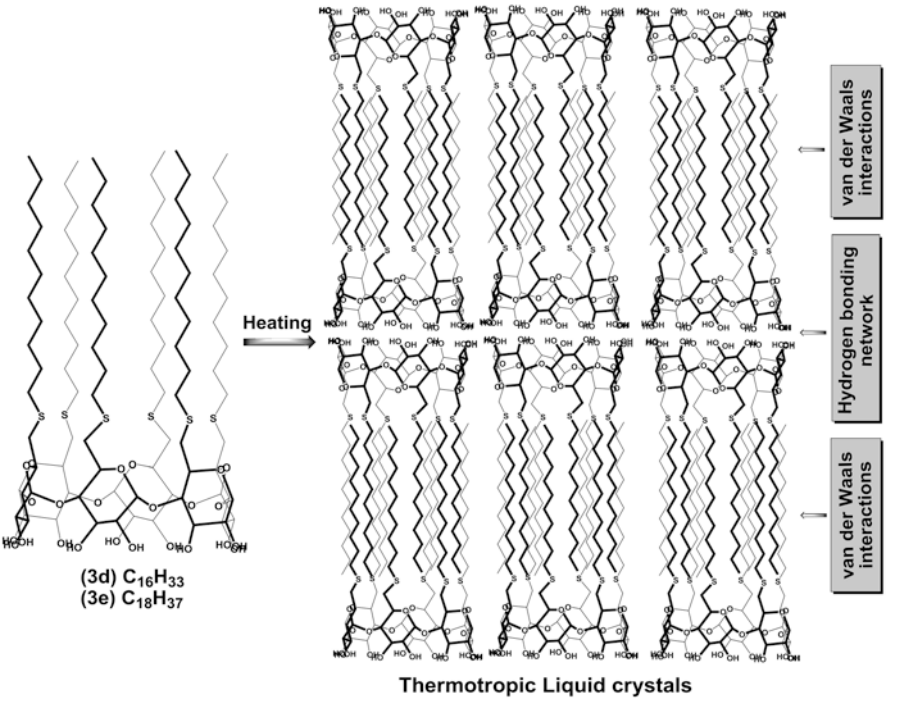

Fig. 7.10 Schematic structures of synthesized β-cyclodextrin derivatives exhibiting thermotropic liquid crystal properties by Ling et al.

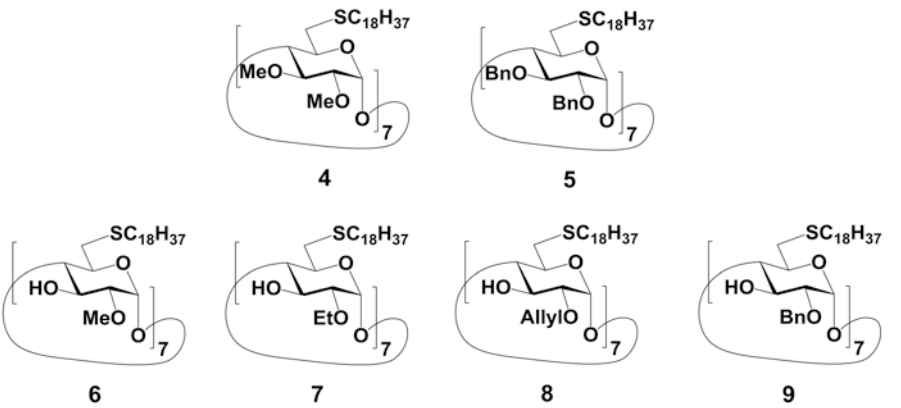

Fig. 7.11 Synthesized per-6-substituted β-cyclodextrin derivatives containing *n*-octadecylthio groups

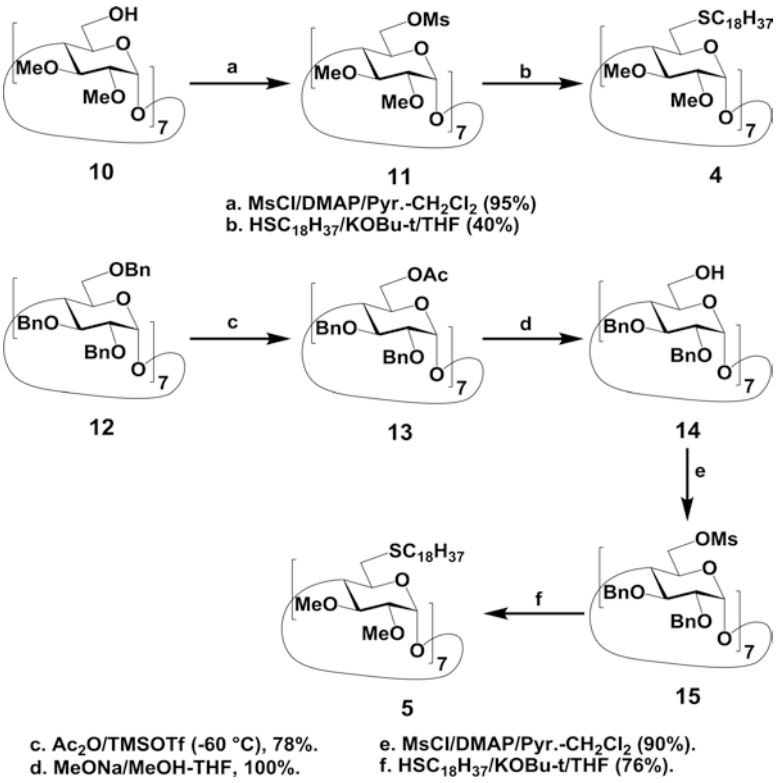

Fig. 7.12 Schematic synthesis of per-6-octadecylthiolated β-cyclodextrin derivatives **4** and **5**

how close the molecules in the bilayers could get to each other in solid state. Logically, the ability to engage intermolecular H-bonding network in solid state should decrease from compounds **6** to **9**.

Compound **4** was synthesized by first mesylating the per-2,3-di-*O*-methylated β-cyclodextrin **10** in a mixture of anhydrous pyridine-dichloromethane to obtain desired per-6-mesylate **11** in 95% yield. Subsequent nucleophilic substitutions of the 6-mesylates with potassium *n*-octadecylalkylthiolate, generated in situ by mixing *n*-octadecylalkylthiol with potassium tert-butoxide (KOBu-t) in THF afforded the desired β-cyclodextrin derivative **4** in 40% yield. The synthesis of the analogous compound **5** started from the per-2,3,6-*O*-benzylated compound **12**, which was first subjected to an acetolysis at −60 °C in acetic anhydride using trimethylsilyl trifluoromethanesulfonate (TMSOTf) as the catalyst; this elegantly converted the less sterically hindered 6-*O*-benzyl groups to the corresponding 6-*O*-acetates in a highly regioselective manner to afford compound **13** (78%). Subsequent Zemplén *O*-transesterification in anhydrous methanol-tetrahydrofuran mixture using sodium methoxide as a catalyst, produced the heptol **14** quantitatively. Compound **14** was then activated in a similarly manner as compound **11** to afford the per-6-mesylate **15** (90%, yield), which was ultimately converted to target compound **5** (76% yield).

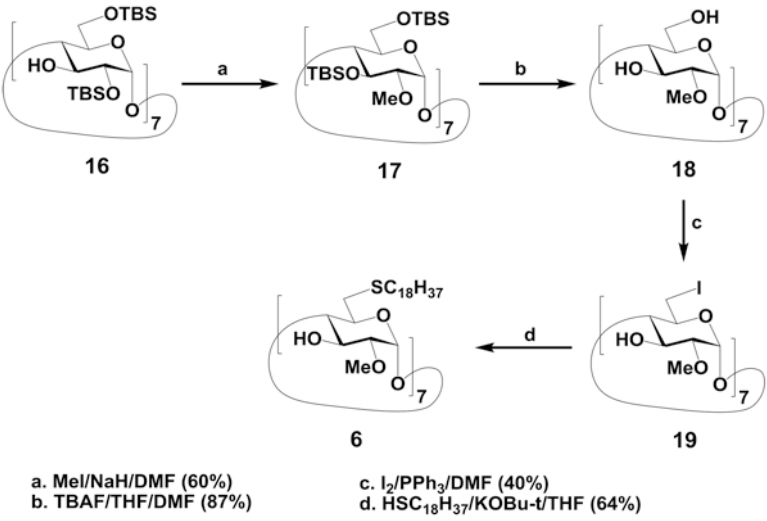

Fig. 7.13 Synthetic scheme of per-6-*n*-octadecylthio-2-*O*-methyl-β-cyclodextrin derivative **6**

Compound **6** was synthesized by reacting a per-2,6-di-*O*-silylated derivative of β-cyclodextrin **16** with methyl iodide in the presence of sodium hydride in anhydrous dimethylformamide (Fig. 7.12) (Fügedi 1989). After the deprotonation, the O2-silyl groups underwent a clean migration to O3-positions of β-cyclodextrin, which provided the opportunity for O2 to be methylated under Williamson etherification conditions. The corresponding compound **17** was isolated in 60% yield (Ashton et al. 1995). The protecting tert-butyldimethylsilyl groups were then removed using tetra-*n*-butylammonium fluoride (TBAF) to obtain polyhydroxylated β-cyclodextrin **18** (87% yield). A regioselective per-6-iodination was then performed using I_2/PPh_3 as a reagent to afford the corresponding per-6-iodide **19** in 40% yield. Finally, all the 6-iodides were substituted by *n*-octadecylthiolate to provide the desired β-cyclodextrin derivative **6** in 64% yield (Fig. 7.13).

The remaining three compounds **7**, **8** and **9** were synthesized according to Fig. 7.14 using compound **20** as a common starting material. First, a regioselective O2-alkylation was performed using NaH as a base, and either ethyl iodide, or allyl bromide or benzyl bromide as an electrophile. The corresponding intermediates **21**–**23** were obtained in 30–52% yields. Then the 6-*O*-*tert*-butyldimethylsiloxy groups were directly converted to the corresponding 6-bromide using homologuous brominating conditions as reported for **19** (bromine/triphenylphosphine in anhydrous dichloromethane); this afforded the corresponding per-6-bromides **24**–**26** in 46–94% yields. Final nucleophilic substitutions by *n*-octadecylthiolate afforded the desired targets **7**–**9** in 39–80% yields (Fig. 7.14). All synthesized β-cyclodextrin derivatives were characterized by 1D and 2D NMR experiments as well as MALDI-mass spectrometry.

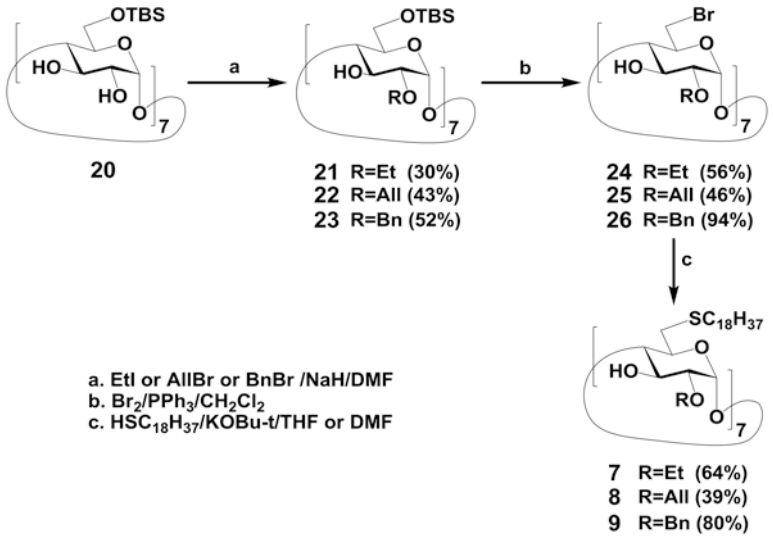

Fig. 7.14 Synthetic scheme of per-6-octadecylthio-2-*O*-alkylated β-cyclodextrin derivatives 7-9

Mesomorphic Properties The mesomorphic properties of β-cyclodextrin derivatives **4–5** were first investigated using differential scanning microscopy to reveal the phase-transitions as well as their associated enthalpic changes. It was found that both compounds **4–5** did not display liquid crystallinity, since only a single phase-transition was observed upon heating, which was attributed to the crystalline-isotropic liquid transition. Thus, clearly, the possible π-π interactions of benzene units present in **5** were not enough to induce long-range ordering in solid states. Interestingly, the two amphiphilic compounds **8**–**9** with larger groups (allyl for **8** and benzyl for **9**) at O2-positons also displayed a single phase transition, as observed by differential scanning calorimetry. This observation was further confirmed by cross-polarized optical microscopy as no birefringence was detected. Thus, both compounds **8** and **9** were found to be incapable of self-assembling into liquid crystalline mesophases, despite the presence of 7-hydroxyl groups. Probably, intermolecular H-bonding network is too weak to induce long-range orders. On the other hand, the two amphiphilic compounds **6** and **7** with smaller alkyl groups (methyl **6** and ethyl **7**) at O2-positions displayed thermotropic liquid crystalline behavior, with the compound **6** being the most mesogenic. From differential scanning calorimetry, compound **6** revealed five endothermic phase transitions upon heating at 50, 60, 64.5, 68, and 110 °C, and four exothermic transitions upon cooling at 95, 56, 40.5 and 37.5 °C (Fig. 7.15). From polarized optical microscope, the heating phase transition observed at 110 °C was associated to the transition to the isotropic liquid phase. However, after cooling to 95 °C, compound **6** displayed fluidity and the characteristic fan-shaped smectic A pattern became increasingly bright and colorful upon further cooling while the material became highly viscous.

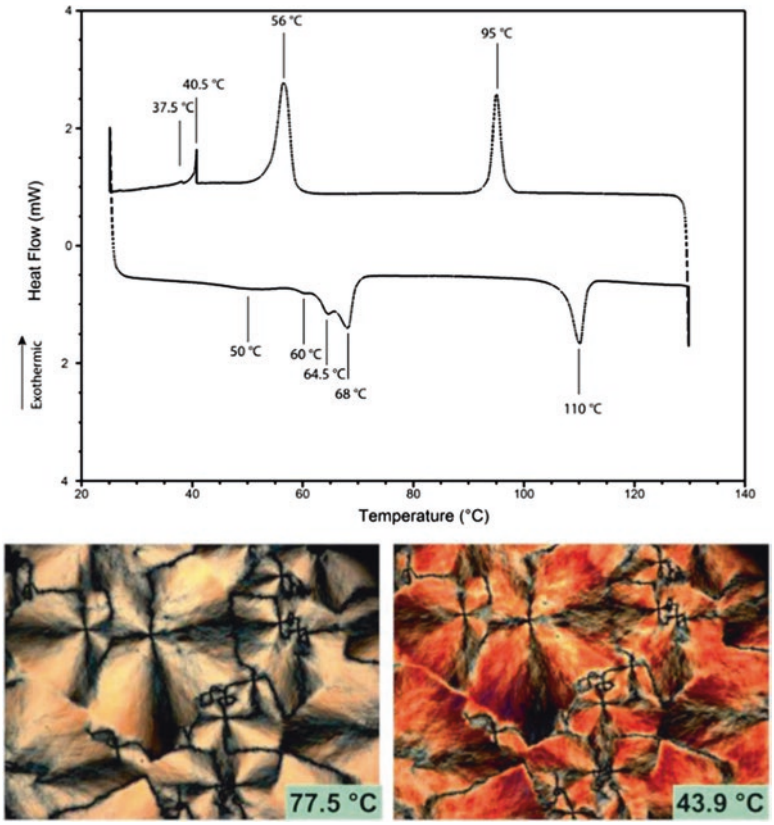

Fig. 7.15 DSC thermogram of compound **6** (Top) and its POM snapshots at 77.5 and 43.5 C (Bottom) "Reprinted with permission from (Ward et al. 2014). *DSC* differential scanning calorimetry, *POM* cross-polarized optical microscopy. Copyright 2014 Royal Chemical Society

On the other hand, compound **7** which had seven O2-ethyl groups - just one carbon longer than the O2-methyl groups in **6** and one carbon shorter than the O2-allyl group in **8**, displayed only two broad endothermic transitions at 54 and 61 °C upon heating, three broad and unresolved exothermic transitions at 43.5, 49 and 51.5 °C during the cooling cycle from the differential scanning calorimetry thermogram (Fig. 7.16). The heating transition observed at 61 °C was determined to be the clearing point of the material into isotropic liquid by cross-polarized optical microscopy. Upon cooling, the characteristic fan-shaped texture of smectic A gradually appeared, but the domains formed were generally much smaller than those of compound **6**, suggesting weakening ability for compound **7** to self-assemble.

Powder X-ray analysis was carried out for compound **6** which confirmed the presence of long range order in the smectic phase. For example, a bilayer thickness of 40.7 Å was determined; this value is significantly smaller than the calculated length (62.2 Å) of head-to-head dimer, suggesting significant interdigitation of the

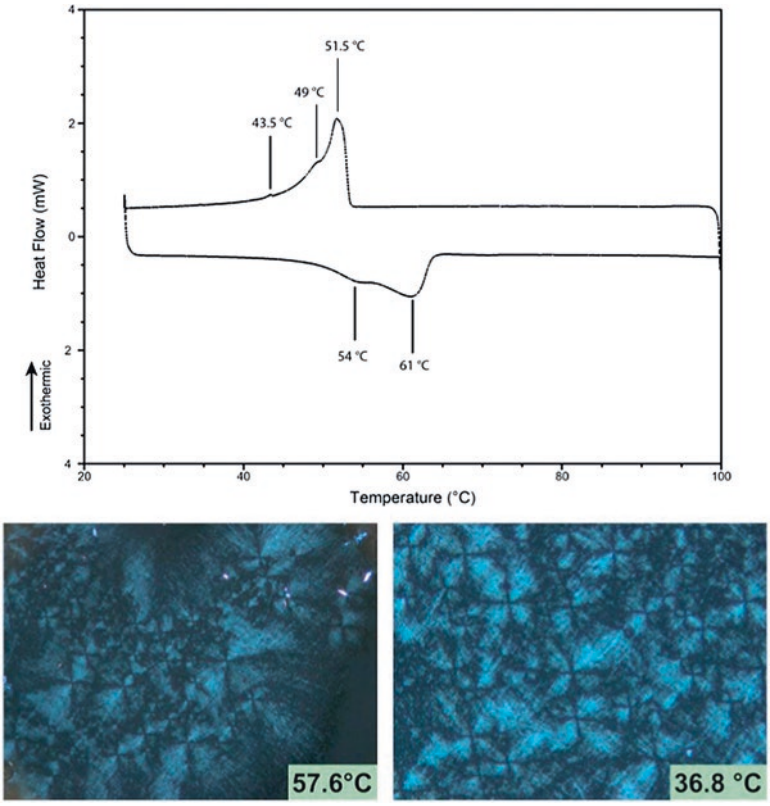

Fig. 7.16 DSC thermogram of β-CD **7** (Top) POM picture at 57.6 and 36.8 C (Bottom) "Reprinted with permission from (Ward et al. 2014). *DSC* differential scanning calorimetry, *POM* cross-polarized optical microscopy. Copyright 2014 Royal Chemical Society

hydrophobic chains in the highly ordered solid states. The presence of broad peaks in the wider angles region were also detected, which suggests the presence of short range orders within the layers at lower temperatures but no distinct phase could be identified. However, the short-range orders disappeared at higher temperatures, as those broad peaks vanished in the determined X-ray diffractograms.

The investigation by Ling and co-workers (Ward et al. 2014) provided great insights on the importance of H-bonding strength on the formation of liquid crystalline mesophases. As can be seen, the per-2-*O*-methyl-β-cyclodextrin **6** had only half number of secondary hydroxyl group compared to compound **3e**, thus intermolecular H-bond network established by compound **6** would be expected to be weaker. This substantially lowered the mesophases temperature (50–110 °C for compound **6** vs 215–280 for **3e**). The ability to form smectic mesophases quickly diminishes from compound **6** to **7** and was completely lost when the chains length attached to O2 reached 3 carbons or longer. A substantially narrower temperature range was observed for compound **7** (range: 54–61 °C) which reflects the transition.

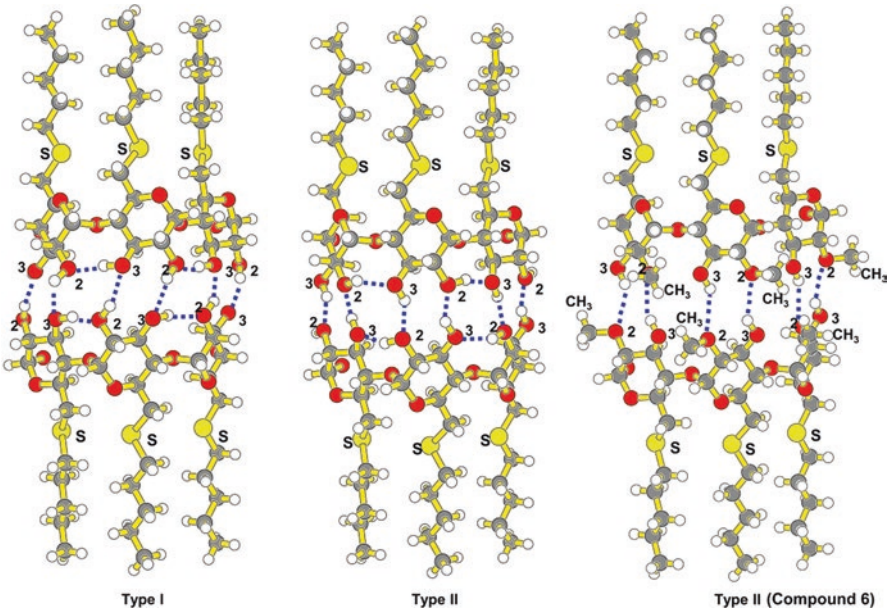

Fig. 7.17 Graphical representation of the two distinct H-bonding networks present in β-cyclodextrin liquid crystals

Previously, through *ab initio* and semiempirical quantum calculation, (Avakyan et al. 2001) proposed models of two types of inter and intramolecular H-bonding networks at the secondary faces of β-cyclodextrin dimers (Fig. 7.17). In type I model, OH-2 groups of one β-cyclodextrin act as H-bond acceptor to the neighboring OH-3 within the same molecule, while the same OH-2 groups simultaneously acts as a hydrogen bond donor to OH-3's of another cyclodextrin molecule. In another type II model, both OH-2's and OH-3's assume a reversed role within inter- and intramolecular H-bond networks. The computational analysis confirmed type I to be thermodynamically preferred as the torsion angle of OH-2 favors the formation of intermolecular H-bonding network. Based on this model, Ling and co-workers found that for both compound **6** and **7**, their per-substitutions at the O2 forbids the formation of the stronger type I network; thus, they concluded that within the mesophases formed by compounds **6** and **7**, type II network was established with OH-3 acting dynamically as H-bond donor through inter and intramolecular interactions within the bilayer. Such model can be effectively used to explain the difference on the clearing point temperatures between compounds **3d/3e** which did not display any clearing point, instead, they slowly decomposed at temperatures above 280 °C, confirming the very strong inter- and intramolecular H-bond networks present in such systems. Conversely, for compounds **6/7**: only weaker inter- and intramolecular H-bond networks could be established. This explains well their lower clearing points at 110 °C and 56 °C for β-cyclodextrin **6** and **7** respectively.

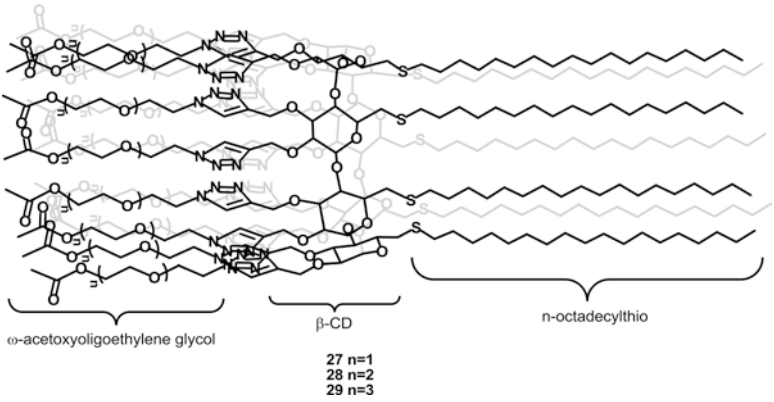

Fig. 7.18 Graphical representation of the stuctrure of cyclodextrin-based liquid crystalline materials **27**–**29** forming smectic mesophases

7.2.1.2 Dipole-Dipole Intermolecular Force Mediated Mesophase Formation Based on Oligoethylene Glycol Functionalized β-Cyclodextrin

For more than a decade, H-bond network was considered to be very important to generate cyclodextrin-based liquid crystals. This intermolecular force has been found to play a crucial role in most published designs of cyclodextrin-based thermotropic liquid crystals (Ling et al. 1993; Shaikh et al. 2007; Yang et al. 2013). Recently, Ling and co-workers (Champagne et al. 2016) reported the first β-cyclodextrin-based liquid crystals (Fig. 7.18, **27–29**) relying on using dipole-dipole interactions as the primary intermolecular force to induce self-assembly. The novelty of their design can be appreciated by the absence of any polar hydroxyl groups, but the presence of 14 *ω*-acetoxy-oligoethylene glycol residues of different lengths (2–4 repeating ethoxy groups) at the secondary face of β-cyclodextrin that are rich with polar C-O bonds. At the primary face, they kept the flexible, apolar *n*-octadecylthio functional groups. Thus, this class of compounds does show amphiphilic properties, but in solid states, due to lack of H-bond donors, the molecules are unable to interact with each other via H-bond network, thus the dipole-dipole interactions between the numerous C-O bonds of the oligoethylene glycol groups would be expected to play the most fundamental role to induce long-range orders in solid states.

Compounds **27**–**29** were synthesized from the per-6-*O*-*tert*-butyldimethylsilyl-β-cyclodextrin **20,** which was first peralkylated at all O2 and O3 positions with propargyl bromide using sodium hydride as base in anhydrous dimethylformamide. The obtained per-2,3-*O*-dipropargylated compound **30** was then subjected to a full *O*-desilylation under acidic conditions (HCl) in a methanol-dichloromethane mixture, to yield desired heptol **31**. After a per-6-mesylation with mesyl chloride in a mixture of anhydrous pyridine and dichloromethane at 0 °C, a highly versatile intermediate **32** was obtained. The alkynic

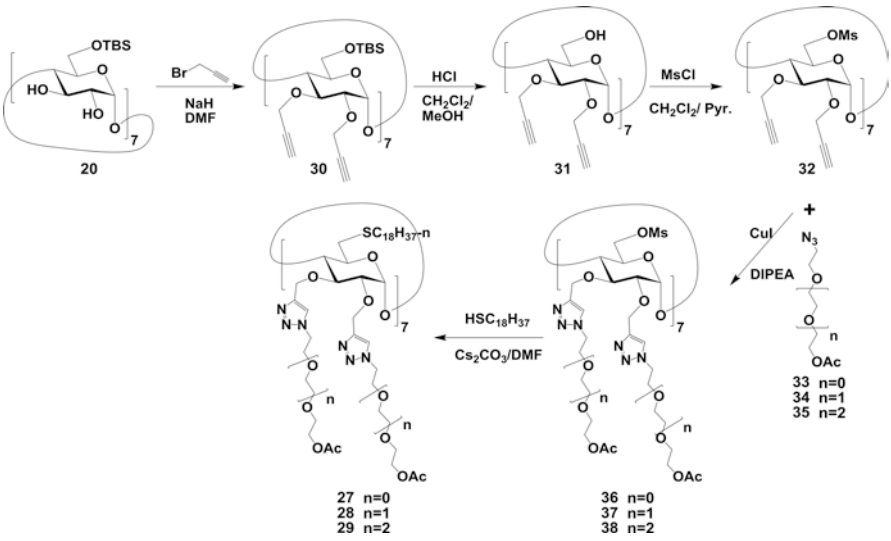

Fig. 7.19 Synthesis of CD-based liquid crystalline materials **27–29** containing polar ω-acetoxyoligoethylene glycol groups

functionalities were subjected to copper(I)-mediated 1,3-dipolar cycloaddition with 3 different ω-acetoxyoligoethylene glycol azides **33–35** of different lengths to obtain the corresponding conjugates **36–38.** The final step involved the nucleophilic substitution of all the 6-mesylates in compounds **36–38** by *n*-octadecylthiolate to afford the desired targets **27–29** (Fig. 7.19).

Thermogravimetric analysis revealed that all compounds **27–29** have excellent thermal stability (up to 283 °C, ca. 5% mass loss). The mesogenic behavior of compounds **27–29** was studied by cross-polarized optical microscopy, differential calorimetry, and powdered X-ray diffractometry. Remarkably, all three derivatives showed strong liquid crystalline properties over a wide range of temperatures. For example, under cross-polarized optical microscopy, compounds **27–29** were observed to clear into isotropic liquid phase at 234.3, 194.8, and 157.7 °C respectively (Fig. 7.20). The compound with the shortest oligoethylene glycol chains **27** cleared at the highest temperature, which was unexpected. Upon slow cooling, all three compounds gradually entered into liquid crystalline phases initially forming small bâtonnet domains that gradually grew and fused into larger bâtonnets which eventually fused together and formed fan-shaped textures. The bâtonnets are commonly observed textures at the transition from the isotropic phase to fluid smectic mesophases. Compared to the mesophases formed via stronger H-bonding network as the intermolecular forces (**3d**-**3d**, **6–7**), Champagne et al. reported much enhanced fluidity for mesophases formed by compounds **27–29**.

Differential scanning calorimetry thermoanalysis revealed a transition at 54.8, 45.9 and 39.3 °C for compounds **27–29**, respectively; they correspond to a relatively large enthalpy change (24.3 Jg^{-1} for **27**, 19.9 Jg^{-1}, for **28**, and 23.3 Jg^{-1} for **29**); the

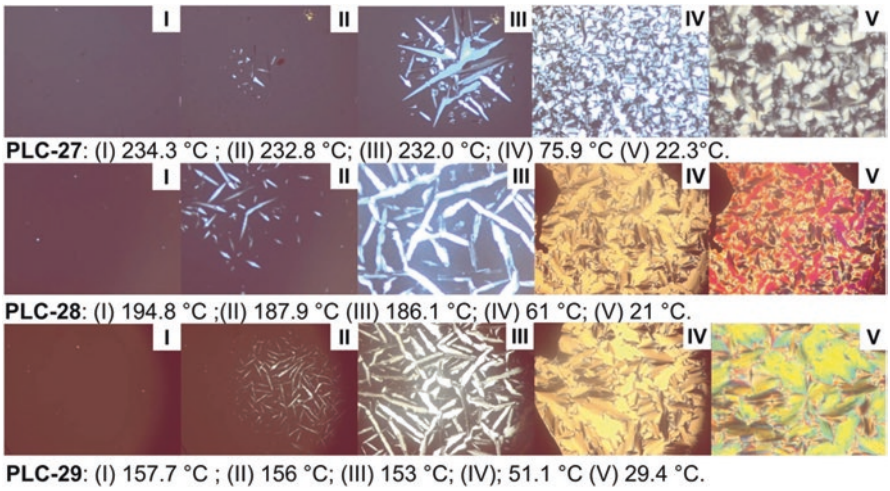

Fig. 7.20 Cross-polarized optical microscopy (POM) images images of β-cyclodextrin **27**–**29** recorded at various temperatures, highlighting their behavior from isotropic transition (I) to room temperature (V)

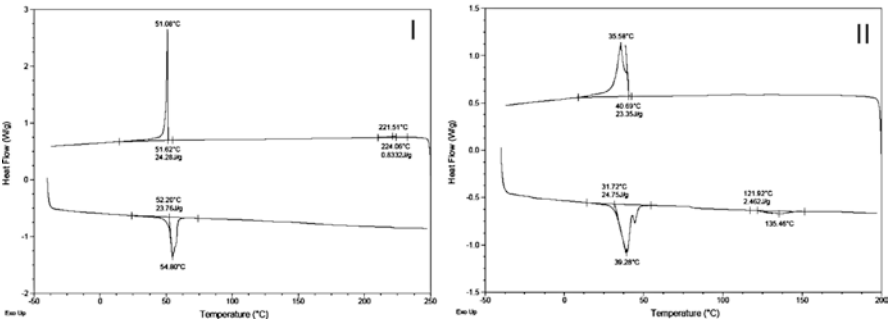

Fig. 7.21 Differential scanning calorimetry (DSC) thermograms recorded for β-cyclodextrin derivatives **27** (I) and **29** (II) as well as the enthalpies associated with the recorded transitions

authors attributed them to the liquid crystalline mesophases to crystalline solid transition for each compound. Thus, all three compounds **27**–**29** form mesophases over an extremely wide range (179.5 °C for **27**, 148.9 °C for **28**, and 118.4 °C **29**), which is remarkable, making this class of compounds unique. On the other hand, differential scanning calorimetry also revealed very small enthalpic variations (< 2.5 Jg^{-1}) for all three compounds **27**–**29** ascribed to the liquid crystalline-isotropic liquid transitions (Fig. 7.21). These enthalpic changes are much smaller when compared to the values associated with previously reported systems that relied on H-bond network (**3d**-**3e**, **6**–**7**). For instance, compound **6** has an enthalpy change of ~19–20 Jg^{-1} corresponding to its isotropic liquid-smectic liquid crystal phase transition. The higher fluidity, lower clearing temperature, and better thermostability are

attributed to the absence of stronger H-bonding network. All these also contributed to the improved liquid crystalline properties of compounds **27–29**.

Solid state Molecular Packing Properties
Champagne et al. reported the powder X-ray diffractograms of **27**–**29** at 20 °C and 50 °C below their respective clearing point. Sharp peaks were observed in the low angle region for all three compounds, corresponding to layer spacing of 55–60 Å, confirming the formation of bilayer structures for all three compounds. This suggested that all three compounds formed smectic liquid crystalline mesophases. On the other hand, broad peaks were also observed in the higher angle region at higher temperatures, which was attributed to a lack of high intra-layer orders. However, when the X-ray diffractograms of compounds **27** and **29** were recorded at room temperature, the peaks in the higher angle region became significantly sharper, which suggested higher positional order within the layers.

Figure 7.22 shows molecular models of packing patterns for compounds **27**–**29**. All three compounds have a conical geometry with calculated length of the molecules varying between 43.6–51.4 Å. The X-ray diffraction data revealed a periodicity much shorter than twice the molecular length in each case, suggesting significant interdigitation in solid states for each compound. Based on the wedge-shaped geometry of each derivative, the authors believed the interdigitation occurs at the hydrophobic chain region (primary face).

7.2.2 Thermotropic Liquid Crystals Based on Cyclodextrin Derivatives Containing Conventional Mesogenic Groups

Mesogens consist of a group of organic compounds that strongly induce liquid crystallinity. These are often rigid molecules such as cholesterol, biphenyl, triphenylene that adopt the shape such as rods, disks etc. When chemically modified with flexible chains, their derivatives usually exhibit mesogenic behavior. Although cyclodextrin molecules represent a class of relatively rigid scaffolds, their mesogenic properties appear to be quite weak. For example, all compounds **4**, **5**, **8**, and **9** did not show any liquid crystalline properties, despite the incorportation of several long alphatic chains at the primary face of the molecules. However, several research groups have reported examples of cyclodextrin-based liquid crystals by incorporating commonly known mesogenic groups to a cyclodextrin scaffold, and the obtained compounds usually displayed mesophases other than smectic.

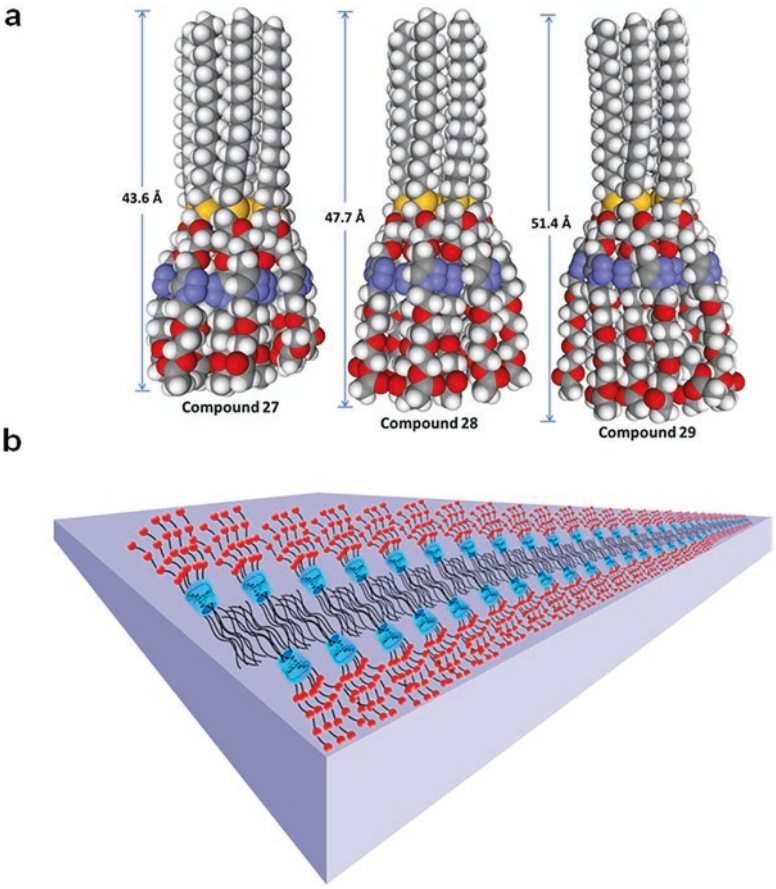

Fig. 7.22 (a) Corey-Pauling-Koltun models displaying the inherited wedge-shaped geometry of compounds **27**–**29,** with a length of 43.6, 47.7 and 51.4 Å respectively, in extended conformation. (b) Proposed model of smectic packing in solid states for all three compounds, with interdigitation at the hydrophobic chain regions

7.2.2.1 Amphiphilic Cyclodextrin Derivatives Containing Cholesterol Residues

Shaikh et al. (2007) reported a first example of amphiphilic β-cyclodextrin-based thermotropic liquid crystal in 2007 by covalently linking β-cyclodextrin to mono-cholesteryl succinate **39** (Fig. 7.23). The synthesis began with an esterification of cholesterol **40** with succinic anhydride in presence of pyridine; this afforded the corresponding cholesterol succinate **41** with a free carboxylic acid. The available carboxylic acid was then activated with thionyl chloride to obtain the corresponding succinyl chloride **42**, which was subsequently used to esterify β-cyclodextrin in anhydrous dimethylformamide at approximately 70 °C for 72 h. The β-cyclodextrin

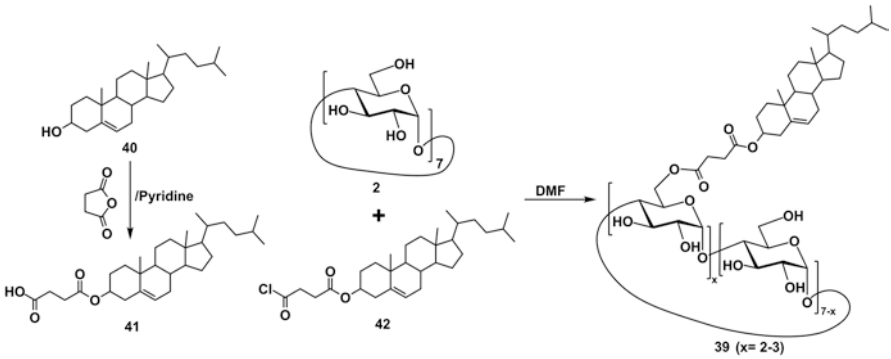

Fig. 7.23 Synthesis of cholesterol appended β-cyclodextrin liquid crystal derivatives **39**

derivative **39** was obtained, unfortunately as a mixture. The degrees of cholesteryl substitution were estimated to be ~2–3, and most substitutions probably occurred at the primary face of the β-cyclodextrin, due to the higher nucleophilicity of OH-6 groups.

The thermotropic mesomorphic behaviour of product mixture **39** was investigated by the authors using various techniques, including Fourier-transform infrared spectroscopy, NMR, differential scanning calorimetry, and cross-polarized optical microscopy. The mixture exhibited birefringence above 130 °C (first heating), and became isotropic at about 180 °C. The differential scanning calorimetry thermogram showed a transition at 120–125 °C associated to the glass-liquid transition. This was well compared to native β-cyclodextrin, which does not exhibit any liquid crystalline properties and was reported to be stable up to 299 °C without experiencing any significant mass loss (Song and Xu 2008; Song et al. 2008). The cross-polarized optical microscopy analysis revealed unclear textures which were not fully characterized. Nevertheless it was interesting to see the synthesized materials displayed birefringence, even with such a low degree of substitutions. Cholesterol is known to induce cholesteric mesophases, thus the liquid crystalline properties of compound **39** was clearly due to the incorporation of cholesterol residues to β-cyclodextrin, and this had significantly reduced the strength of both the inter- and intramolecular H-bonding network of the materials in solid states.

7.2.2.2 Amphiphilic Cyclodextrin Derivatives Containing 4-methoxybiphenyl Residues

Chen et al. (2010) reported another amphiphilic β-cyclodextrin derivative **43** (Fig. 7.24) that was modified with a hydrophobic tail derived from the propargyl 6-(4′-methoxybiphenyl-4-yloxy)hexanoate group **46** at all the primary positions. The efficient copper (I)-mediated 1,3-dipolar cycloaddition was used to complete the hydrophobic modification of β-cyclodextrin core via the per-6-azide intermediate **45** in dimethylformamide. Thus, in the final molecule **43**, Chen et al.

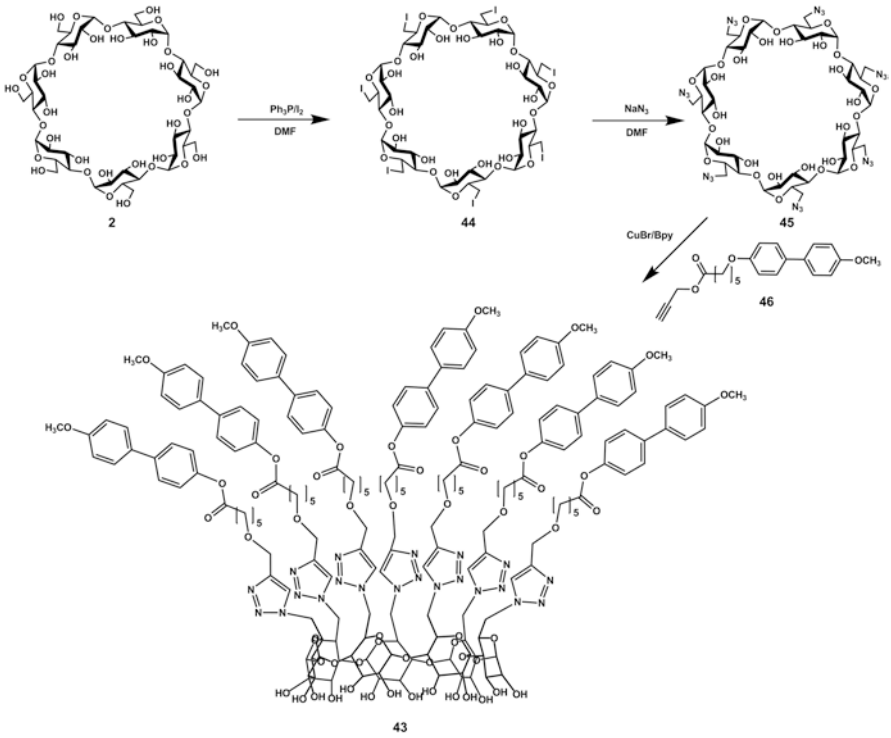

Fig. 7.24 Synthesis of cyclodextrin-biphenyl thermotropic liquid crystal **43** forming smectic mesophases

incorporated 7 copies of 4′-methoxybiphenyl group which is known to induce liquid crystallinity because of its rigidity and rode-like geometry. In solid states, the 4′-methoxybiphenyl groups can interact with each other via π-π interactions. The purity of the final compound **43** was verified by ^{1}H NMR spectroscopy, Fourier-transform infrared as well as MALDI-TOF mass spectrometry.

Thermogravimetric analysis revealed the amphiphilic compound was quite stable at high temperature, as only a loss of 5% mass was observed at 318.5 °C. Differential scanning calorimetry thermoanalysis showed several phase transitions. For example, during the second heating cycle, endothermic transitions at 130.1 °C, 188.7 °C and 217.2 °C were observed with the last one correlating to the clearing temperature to isotropic liquid. Using cross-polarized optical microscopy, the birefringent properties of compound **43** were investigated, which revealed very interesting patterns. For example, at 50 °C, fan-shaped textures were observed, which transition into conic focal patterns at 180 °C and subsequently into schlieren lines at 195 °C that persisted until the material completely cleared into isotropic phase at 230 °C. The ability to form various mesophases revealed the great self-assembly ability of compound **35**. This also differentiates it from other amphiphilic cyclodextrin derivatives that show liquid crystallinity.

Wide angle X-ray diffractometry was used to analyze the mesophases formed by compound **43**. At 30 °C, 3 peaks in the small-angle region were observed with q ratios of 1:2:3; this allowed the authors to assign the structure of formed mesophase to be lamellar. In the wide-angle region, 3 peaks were also observed with 1 very strong, 1 strong, and 1 weak. Based on the characteristic patterns, Chen et al. concluded that compound **43** formed highly ordered smectic E mesophase at low temperatures. At 160 °C, the material showed similar diffraction patterns at the low-angle region (virtually unchanged), suggesting that the layered smectic structure was maintained. However, peaks in the wide-angle region did become broader, suggesting a slow transition to smectic A mesophase (Koltzenburg et al. 1998). Upon increasing temperature further to 200 °C, wide angle X-ray diffractometry detected no peaks within the low angle region, while only a diffused halo appeared in the high-angle region, corresponding to a phase transition to nematic phase: losing the layered structures (Dong et al. 2004). The material eventually entered its isotropic liquid phase at ~230 °C. Figure 7.19 depicts the proposed self-assembled supramolecular packing model of compound **43**. As can be seen, the strongest intermolecular force that dictates the molecules to self-assemble was the H-bonding network occurring at the secondary face of β-cyclodextrin, resulting in dimerization. Such network persists from room temperature to the high clearing point into isotropic liquid state thus is responsible for the formation of lamellar structures in solid states. The lamellar organization of molecules is further promoted by the 4′-methoxybiphenyl units which interact with one another via intermolecular π-π-interactions. Chen et al. proposed that 3 or 4 of the biphenyl mesogenic units were oriented in opposite directions with respect to the primary face of the β-cyclodextrin; this adds a second level of orders that are responsible for formation of smectic E mesophases. The π-π-interactions between the 4′-methoxybiphenyl units became significantly disrupted at higher temperatures (during the smectic A and nematic phases). The authors confirmed such mode of organization through molecular modelling. For example, the calculated *d* spacing between opposing 4′-methoxybiphenyl units at the primary face of β-cyclodextrin is 38.6 Å, which matches almost perfectly the determined *d* spacing of 38.4 Å by wide angle X-ray diffractometry at room temperature (Fig. 7.25).

7.2.2.3 Cyclodextrin Derivatives Containing a Triphenylene Mesogenic Group

In 2013, another β-cyclodextrin-based thermotropic liquid crystal was reported (Yang et al. 2013). The authors conjugated a mesogenic triphenylene group to a β-cyclodextrin scaffold (Fig. 7.26). Triphenylene derivatives represent one of the most widely studied discotic mesogens due to their potential applications in many areas including light-emitting diodes, organic photovoltaic cells, organic field-effect transistors, gas sensors, and photocopying machines (Zhang et al. 1992; Kumar 2004; Kato et al. 2006; Laschat et al. 2007; Sergeyev et al. 2007; Cammidge and Gopee 2009). The synthesis began with a monotosylation of β-cyclodextrin under

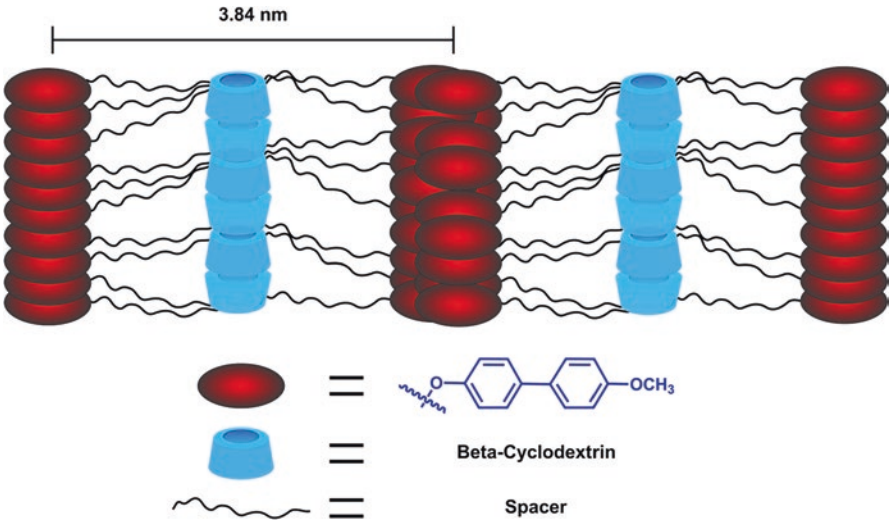

Fig. 7.25 Suggested lamellar organization of compound **43** in the smectic E mesophases

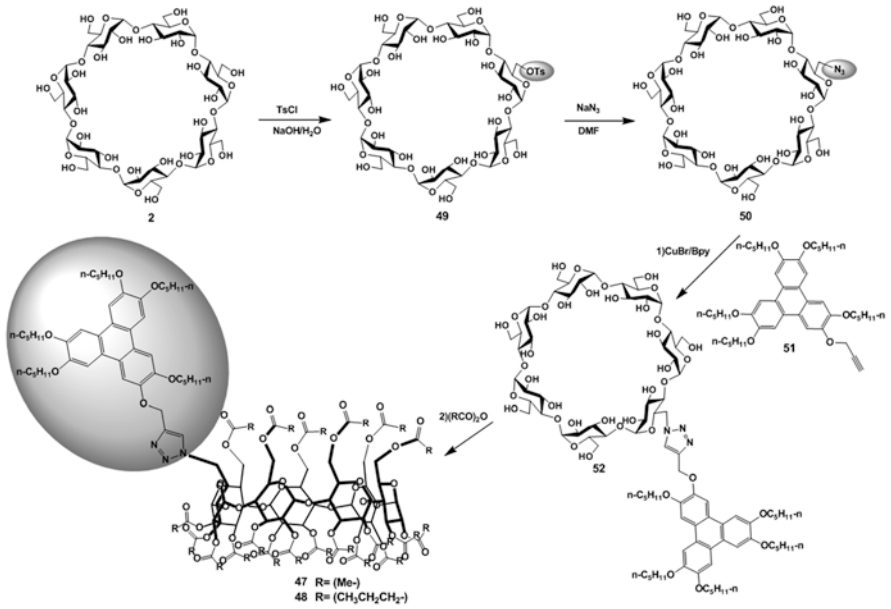

Fig. 7.26 Synthetic scheme of triphenylated-β-cyclodextrin columnar liquid-crystalline materials

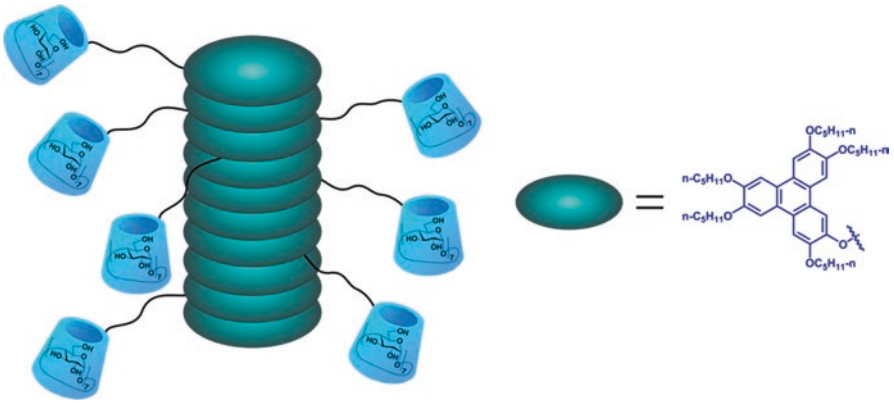

Fig. 7.27 The proposed columnar packing model of triphenylene-β-cyclodextrin conjugate **47**

basic conditions (aqueous NaOH) to obtain compound **49**, followed by a conversion to monoazide **50** in a mixture of dimethylformamide and water, and subsequently, conjugation with triphenylene derivative **38** containing five flexible *O*-n-pentyl chains and one *O*-propargyl group via the copper (I) promoted 1,3-dipolar cycloaddition. The obtained amphiphilic triphenylene-β-cyclodextrin conjugate **52** was then investigated using cross-polarized optical microscopy, but unfortunately, no mesophase was identified. In fact, compound **52** slowly decomposes without transitioning into isotropic liquid. Compound **52** was subsequently esterified, with acetic anhydride or *n*-butanoic anhydride, to afford the corresponding non-amphiphilic conjugates **47** and **48** respectively.

Interestingly, using cross-polarized optical microscopy, only the per-*O*-acetylated compound **47** was found to display mesogenic properties, with the characteristic fan-shaped textures associated to columnar mesophase observed (Prasad et al. 2003; Wan et al. 2003; Ba et al. 2003; Paraschiv et al. 2007). The more flexible compound **48** did not exhibit any birefringence upon heating, as a direct transition from solid state to isotropic phase was observed. For compound **47**, Differential scanning calorimetry only revealed two transitions upon heating at 115.2 °C and 160.4 °C, which correspond to crystalline-columnar mesophase-isotropic liquid transitions.

X-ray powder diffraction pattern of cyclodextrin derivative **47** revealed characteristic patterns of a triphenylene-based columnar mesophase. Peaks at the low angle and high angle regions were observed, and corresponded to the diameter of the columnar triphenylene groups (16.8 Å), the average distance of the molten alkyl chains (4.9–3.7 Å) and the intracolumnar spacing (3.6 Å). Yang et al. concluded that the presence of the strong H-bonding network was an obstacle for the formation of cyclodextrin-based liquid crystals. This H-bond network was eliminated through esterification, thus providing the molecules with the ability to self-assemble via π-π-interactions through the triphenylene moieties. However, the roles of β-cyclodextrin played during mesophase formation appear to be less important (Fig. 7.27).

7.2.3 *Polymeric Cyclodextrin-Based Thermotropic Liquid Crystals*

Recently, liquid crystalline polymers have received considerable attention due to their potential use as biomedical materials, photoelectric materials, switches, smart and stimuli responsive materials (Verploegen et al. 2009; Kim et al. 2014; Wang et al. 2014; Gündüz 2015; Mamiya et al. 2015). Liquid crystal polymers containing cyclodextrin molecules are of particular interests because of their cavities which can be used for host guest interactions with different properties. There have been two types of cyclodextrin-based liquid crystalline polymers reported in the literature so far: the first is related to cyclodextrin-based star-shaped polymers and the second is related to cyclodextrin-based rotaxane polymers.

7.2.3.1 Cyclodextrin-Core Star-Shaped Thermotropic Liquid Crystals

In 2009, He and co-workers (He et al. 2009) reported the synthesis and characterization of an α-cyclodextrin-based star-shaped polymer via atom transfer radical polymerization. Owing to circular geometry and multivalent functionality (18–24 hydroxyl groups), cyclodextrin molecules possess great potential to be used as scaffold to generate star-shaped polymers (Ohno et al. 2001; Stenzel-Rosenbaum et al. 2001; Karaky et al. 2005). Materials of such kind could find applications as switchable windows, displays, color projectors, and other electric-optical systems (Doane et al. 1986; Lin et al. 1995; Bouteiller and Barny 1996; Petti et al. 2003; Serhatli and Kacar 2006). Azobenzene is the moiety that attracted the utmost interest due to its reversible photoisomerization (Han et al. 2006). To synthesize the desired copolymer, α-cyclodextrin was first esterified with 2-bromoisobutyryl bromide, to generate a star-shaped core (incomplete substitutions were recorded, average degree of substitution: 13) containing numerous radical initiating sites; which was subsequently polymerized with a previously synthesized methacrylate derivative containing a flexible hexyl chain terminated with a 4-methoxy-4-oxy-azobenzene mesogenic group. The radical polymerizations were mediated by CuBr/Spartein using four different ratios of monomer methacrylate vs α-cyclodextrin core. All synthesized polymers showed a polydispersity index of approximately 1.5.

The thermotropic liquid crystalline properties of the synthesized materials were investigated and they all displayed both smectic-nematic phase transitions. The observed temperatures associated with smectic to nematic as well as nematic to isotropic phase transitions increased with molecular weights. For instance, the polymer obtained from combining methacrylate: α-cyclodextrin core of 60:1 was observed to display characteristic schlieren nematic textures after being heated to isotropic liquid and subsequently cooled below 125 °C; further cooling to 80 °C yielded the representative smectic textures.

The photoresponsive behavior of the material was investigated in tetrahydrofuran by UV-Vis spectroscopy. After irradiation at 360 nm, the intensity of the π→π* transition band decreased, which contrasted with a noticeable increase of the n→π* transition. The complete isomerization of the azobenzene moieties was observed after irradiating the sample for 5 min. As expected, the reverse trans-cis isomerization happened thermally and /or photochemically in which the trans isomer being thermodynamically favored by approximately 48 kJ/mol (Corruccini and Gilbert 1939).

7.2.3.2 Polyrotaxane-Based Thermotropic Liquid Crystals

Polyrotaxanes consist of a class of supramolecular polymers that have non-covalently linked cyclic organic structures such as cyclodextrins or crown ethers, threaded on a linear polymer such as polyethylene glycol chains. The cyclic molecules are mechanically locked with the threading polymer by bulky caps placed at each end of linear polymer (Gibson et al. 1994). Since their synthesis was first reported by Harada et al. in 1992, polyrotaxanes have attracted a considerable interest from the research community (Harada et al. 1992). One of their most interesting properties is the ability of cyclic structures to rotate and slide over the linear polymer chain. This feature allowed the preparation of fascinating materials such as molecular tubes, obtained by cross-linking macrocycles onto a single thread (Harada et al. 1993). Polytotoxanes have also found various applications (Okumura and Ito 2001) in designing stimuli-responsive properties such as antiscratching, self-healing (Noda et al. 2014), pressure sensitive drug releasing systems (Katsuno et al. 2013). The advantages of designing liquid crystalline materials based on polyrotaxanes are the absence of covalent linkages, resulting in materials with great fluidity, a useful parameter in thermotropic liquid crystals.

In 2007, Ito et al. (Kidowaki et al. 2007) reported a very interesting polyrotaxane-based thermotropic liquid crystal based on α-cyclodextrin. In their design, they conjugated a derivative of hexanoyl chloride which was functionalized with a mesogenic 4′-cyanobiphenyl residue at the end of the chain, to a rotaxane, pre-formed by threading α-cyclodextrin onto polyethylene glycols. 1-Amdantanamine was used as the cap for the polyrotaxane due to its unusually high binding affinity to α-cyclodextrin (Cromwell et al. 1985; Eftink et al. 1989; Gelb and Schwartz 1989; Palepu and Reinsborough 1990; Kwak and Gomez 1996; Harries et al. 2005). The average molecular weight of the rotaxane was ~35,000 (~110 copies α-cyclodextrin per thread) which represented ~28% coverage of the polyethylene glycol axis. Figure 7.26 shows a schematic representation of the synthesized polyrotaxane polymer. Using ^{1}H NMR spectroscopy, it was estimated that about 42% of the hydroxyl groups of α-cyclodextrin reacted with the hexanoyl chloride derivative, which translates into approximately 7.6 cyanobiphenlyl units per α-cyclodextrin (Fig. 7.28).

Differential scanning calorimetry revealed one endothermic transition at 136 °C upon heating, and two exothermic transitions respectively at 70 and 129 °C upon

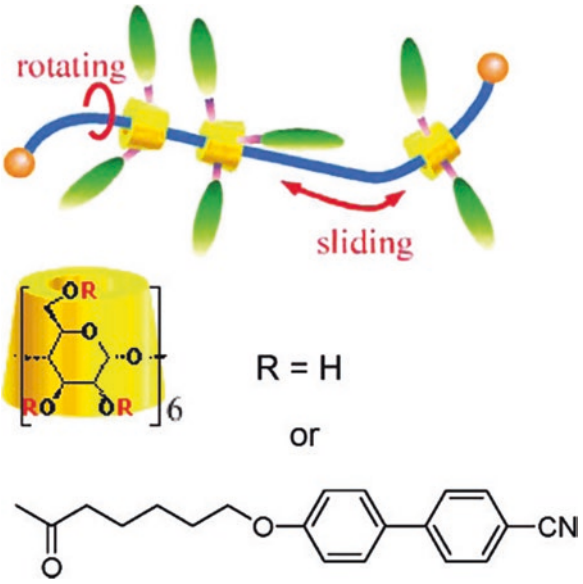

Fig. 7.28 Schematic representation of 6-(4′-cyanobiphenyl-4-yloxy)hexanoyl-functionalized polyrotaxanes based on α-cyclodextrin. "(Kidowaki et al. 2007)". Copyright 2007 American Chemical Society

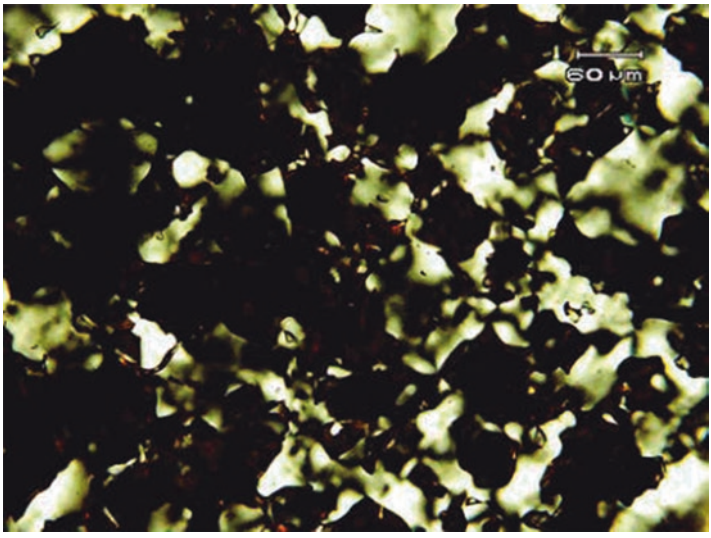

Fig. 7.29 Schlieren-like texture observed for 6-(4′-cyanobiphenyl-4-yloxy)hexanoyl-functionalized polyrotaxanes. "(Kidowaki et al. 2007)". Copyright (2007) American Chemical Society

cooling. The phase transition at 70 °C was attributed to a glass transition while the phase transition at 129 °C was attributed to the biphenyl mesogenic side chains.

Using cross-polarized optical microscopy, schlieren-like texture was observed at 100 °C, indicating the presence of a nematic mesophase (Fig. 7.29). The brightness of the texture gradually increases with decreasing temperature, and were preserved

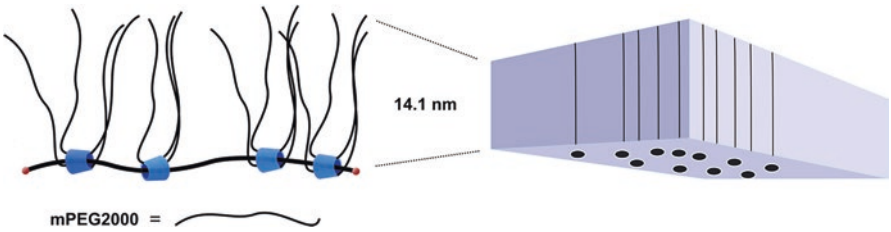

Fig. 7.30 Schematic representation of formed smectic A mesophases by α-cyclodextrin-based polyrotaxane grafted with mPEG2000 chains. The free sliding and rotation of each mPEG2000 grafted α-cyclodextrin subunit on the polyethylene glycol axis facilitates the self-organization of the mPEG2000 side chains into large organized domains

at room temperature which is indicative of a liquid crystalline glass state at ambient temperature. X-ray diffraction patterns measured at 25, 80 and 180 °C further confirmed the presence of a nematic mesophase at temperatures below 130 °C.

Following the work of Ito et al., Araki and co-workers (Araki et al. 2014) later reported another α-cyclodextrin-polyrotaxanes-based thermotropic liquid-crystal by simply grafting mPEG2000 dicarboxylic acid to similar polyrotaxne as above, using 1,1-carbonylbis-1*H*-imidazole as the coupling reagent to obtain polyrotaxane-mPEG2000 copolymer with an estimated 75 copies of mPEG2000 per chain. The authors describe the geometry of their polymer as "sliding graft copolymer" which has a 'rope-curtain like' structure (Fig. 7.28).

Cross-polarized optical microscopy confirmed the fluidity of the material at 65 °C and formation of Grandjean terrace texture, typically associated with the formation of smectic mesophases (Oh 1977; Oswald and Pieranski 2005). On the other hand, X-ray diffraction at ambient temperature revealed several peaks associated with crystalline PEG (Barnes and Ross 1936; Bortel et al. 1979). At temperatures above 65 °C, X-ray diffraction also confirmed the formation of smectic A mesophase with a layer distance of 14.1 nm, corresponding to the predicted contour length of mPEG2000 (13.18 nm). Thus, despite the absence of mesogenic groups, this material was capable of self-organize into smectic A mesophases. The authors attributed the properties of the materials to the one-directional free sliding and rotation of each mPEG2000 grafted α-cyclodextrin subunit on the polyethylene glycol axis (Fig. 7.30).

Additionally, Hu and co-workers (Hu et al. 2011) also prepared a series of α-cyclodextrin-polyrotaxane derivatives conjugated with mesogenic azobenzene moieties by varying the spacer lengths between azobenzene and α-cyclodextrin. Their experimental results suggested that azobenzene-functionalized polyrotoxanes failed to show liquid crystalline behavior with spacer length of 2 and 4 while the analogous polyrotaxanes with spacer length of 6 displayed columnar nematic mesophase. However, when the spacer length was increased to 11, additional high ordered structures were formed by the azobenzene mesogens. Figure 7.31 illustrates a model of molecular organization in solid states for the azobenzene-functionalized polyrotaxanes with a spacer length of 11 carbons (**Azo-PR-11**).

More recently, Guo and co-workers (Guo et al. 2016) reported a new kind of α-cyclodextrin-polyrotaxanes by grafting 4-phenylazobenzoyl moieties directly to

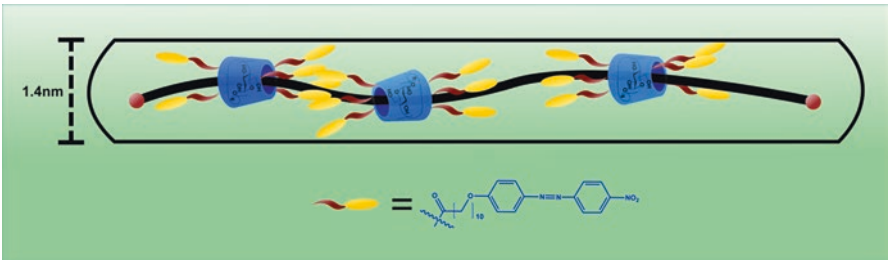

Fig. 7.31 Graphical representation of polyrotaxane Azo-PR-11, molecular arrangement allowing enhanced β-cyclodextrin mobility on the polyrotaxane glycol thread

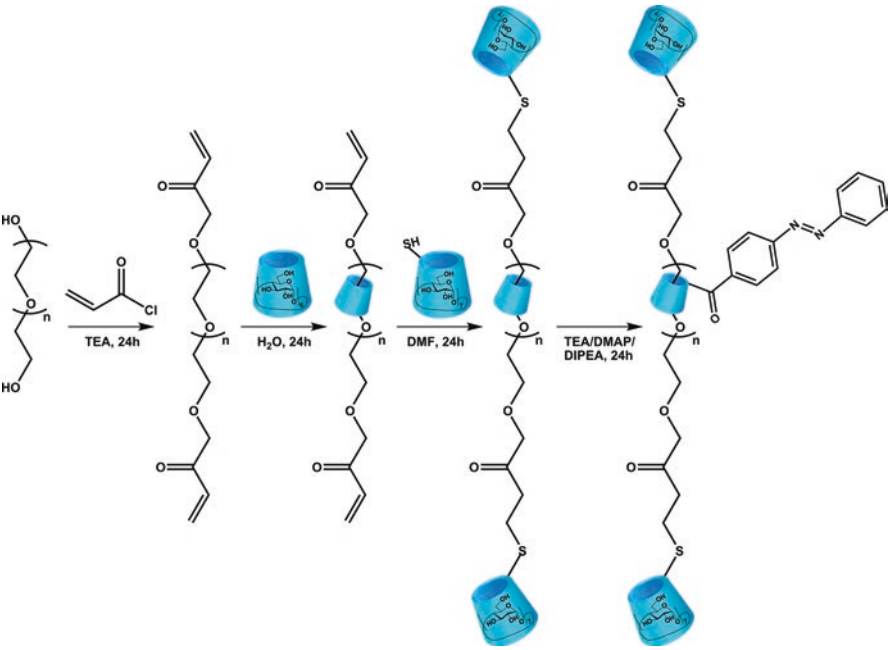

Fig. 7.32 Synthetic scheme of azobenzene-functionalized columnar nematic liquid-crystalline polymeric materials.

cyclodextrin scaffolds without spacer. The parent α-cyclodextrin-polyrotaxane was prepared by mixing vinyl-polyethylene glycol and α-cyclodextrin in aqueous solution and subsequently caped with thiolated β-cyclodextrin. The azobenzene mesogen was then added directly to the free hydroxyl groups of cyclodextrins. The introduction of azobenzene moieties reduces the strength of inter and intramolecular H-bonding networks thus, successfully destruct the channel-like crystalline structure of the parent α-cyclodextrin-polyrotaxane, to provide enhanced mobility/rotation for cyclodextrin subunits on the thread. The introduced mesogenic groups engage intermolecular interactions to induce the thermotropic liquid crystalline behavior of the material (Fig. 7.32).

Cross-polarized optical microscopy revealed schlieren-like textures when the material was heated above 180 °C. In comparison, the parent unmodified α-cyclodextrin-polyrotaxanes did not display liquid crystalline behavior at any temperature. Interestingly, this 4-phenylazobenzoyl-functionalized α-cyclodextrin-polyrotaxane also showed lyotropic liquid crystalline behaviour in dimethyl sulfoxide solution at concentration of 5–0.2 wt%. With the help of wide angle X-ray diffraction patterns, the columnar nematic mesophase of the material was confirmed.

7.3 Cyclodextrin-Based Lyotropic Liquid Crystals

As discussed earlier, amphiphilic cyclodextrin derivatives have excellent ability to self-assemble in solvents, forming different self-assembled systems including lyotropic liquid crystals. In this development, Gulik and co-workers (Gulik et al. 1998) investigated the lyotropic liquid crytstal properties of a class of amphiphilic cyclodextrins, esterified at all secondary hydroxyl groups with acyl chains of different lengths (β-cyclodextrin-C*n*; n = 6, 8, 10, 12, and 14; α-cyclodextrin-C_{14}, and γ-cyclodextrin-C_{14}). Both X-ray scattering and freeze fracture electron microscopy were used in their experiments. The structural analysis of the obtained cyclodextrins revealed that aliphatic chains are stacked similarly to lipid systems and arrange themselves in 2-D hexagonal phases. β-cyclodextrin-C6, -C8, -C10, and -C12 and γ-cyclodextrin-C14 were optically birefringent, while β-cyclodextrin-C14 and α-cyclodextrin-C14 were optically isotropic. X-ray diffractions revealed seven sharp reflections for *β*-cyclodextrin-Cn (n = 6, 8, 10, and 12) with dimensions of 25.9, 30.8, 33.0 and 35.3 Å, respectively. Interestingly, the birefringent materials produced were found to organize into polar columns of 2-D hexagonal lattice. Such results contrasted with *γ*-cyclodextrin-C14 which only displayed broad reflections associated to 2-D hexagonal lattice with dimension of 37.6 Å. On the other hand, *α*-cyclodextrin-C14 and *β*-cyclodextrin-C14 exhibited sharp reflections corresponding to body-centered cubic lattice of optically isotropic materials with dimension of 42.6 Å and 43 Å, respectively. The 2-D hexagonal phase of *β*-cyclodextrin-Cn (n = 6, 8, 10, and 12) and cubic lattice of *α*-cyclodextrin-C14 and *β*-cyclodextrin-C14 were further supported by freeze fracture micrographs (Fig. 7.33A–D). Compounds *β*-cyclodextrin-Cn (n = 6, 8, and 10) in hexagonal phases and *α*-cyclodextrin-C14 and *β*-cyclodextrin-C14 in cubic phases showed ordered and organized domains, respectively while less ordered domains were observed for *β*-cyclodextrin-C12. The polar columns of hexagonal phase comprised of stacked cyclodextrin units in which polar heads were pointed toward the interior of the self-assembled structure, while paraffinic units were projected toward the exterior (Fig. 7.33E). The respective cubic lattice of *α*-cyclodextrin-C14 and *β*-cyclodextrin-C14 consists of 12 molecules per unit cell. It was proposed that the cubic lattice comprised of either polar or paraffinic globules at the center and edges of the cell (Fig. 7.33F, G). The polar globules were comprised of six molecules of *α*-cyclodextrin-C14 or

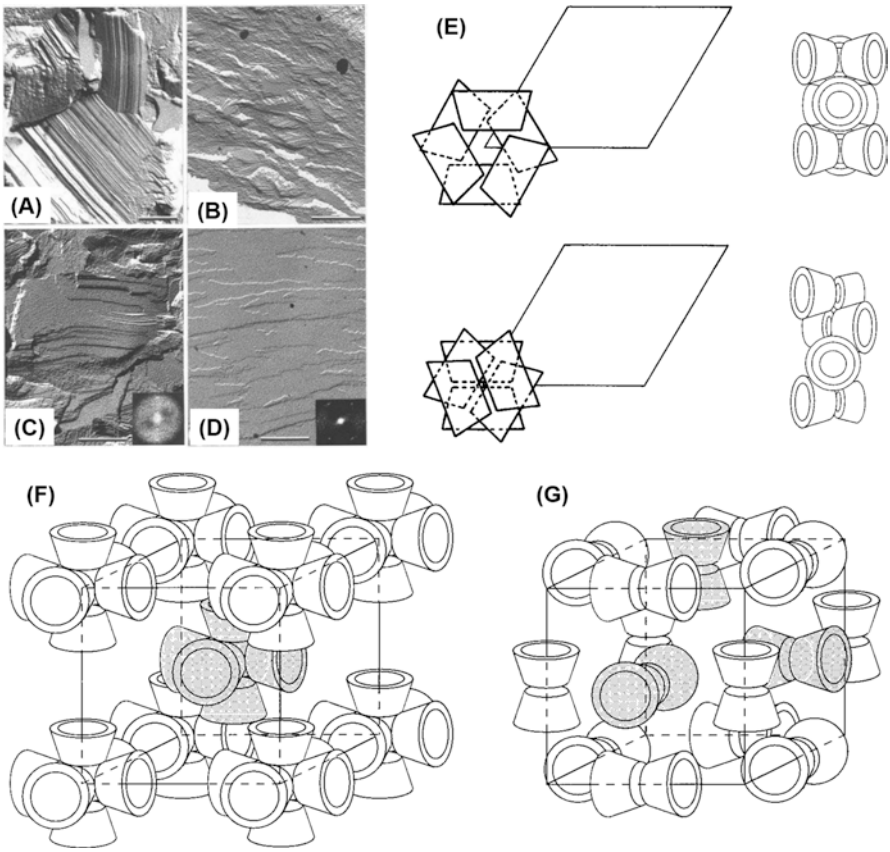

Fig. 7.33 Freeze fracture electron micrographs of (**A**) β-cyclodextrin-C6, (**B**) β-cyclodextrin-C8, (**C**) β-cyclodextrin-C10, (**D**) β-cyclodextrin-C14 (Scale bar = 200 nm). (**E**) Two possible associations of 2D hexagonal structure models with polar columns of stacked cyclodextrin units. (**F**, **G**) The possible cubic structure models of α-cyclodextrin-C14 or β-cyclodextrin-C14 containing either polar (**F**) or paraffinic globules (**G**) at the vertex (in gray color). The paraffinic chains are omitted for clarity. (**A**–**G**) are adapted with permission from (Gulik et al. 1998). Copyright (1998) American Chemical Society

β-cyclodextrin-C14 (Fig. 7.33F) while paraffinic globules consist of dimers of *α*-cyclodextrin-C14 or *β*-cyclodextrin-C14 connected by their primary hydroxyl groups (Fig. 7.33G). The combined analysis of X-ray scattering, freeze fracture electron microscopy, and electron density distribution confirmed the paraffinic globules arrange themselves in the cubic lattice (Fig. 7.33G). The orientation of dimers, while occupying the middle of each edge, was parallel to axis of cubic cell and orthogonal to adjacent dimer. The formation of cubic lattice for such amphiphilic cyclodextrins was found to be unusual and was rationalized by the large surface area of the aliphatic chains.

Cyclodextrins are well known to bind to various types of surfactants by inclusion of their hydrophobic tails into cyclodextrin's cavity. Surfactants are widely used in

daily practical applications including cleaning, emulsifying, detergents, paints, biocides, and insecticides (Rosen and Kunjappu 2012). Upon interactions with cyclodextrins, significant changes occurred in inherent properties and structural dynamics of surfactants. For instance, sodium dodecyl sulfate (SDS), a common surfactant abundantly used in cleaning, cosmetics, and hygiene products, exhibited different self-assembly behavior in the presence of β-cyclodextrin. Sodium dodecyl sulfate forms highly stable water soluble inclusion complexes with two β-cyclodextrin molecules (sodium dodecyl sulfate@2β-cyclodextrin) in 1:1 and 1:2 stoichiometry (Dorrego et al. 2000; Jiang et al. 2011). Generally, sodium dodecyl sulfate@2β-cyclodextrin complexes disfavor self-assembly in aqueous medium due to their hydrophilic outer surface (Saenger and Müller-Fahrnow 1988). However, self-assembled aggregates such as vesicular and lamellar mesophases were observed for sodium dodecyl sulfate@2β-cyclodextrin complex in aqueous solution. To gain deeper insight into such aggregation behavior, the concentration, H-bonds, and electrostatic interactions of the cyclodextrin/sodium dodecyl sulfate complex were investigated. It was observed that by changing the mass concentration of sodium dodecyl sulfate@2β-cyclodextrin complexes, three types of aggregates were formed, including: region I (50–25 wt%), region II (25–6 wt%) and region III (6–4 wt%) (Jiang et al. 2011). In mass concentration range of 50–25 wt%, semi-transparent self-assembled lamellar structures were identified, exhibiting static birefringence observed under cross-polarized optical microscopy, a suggestive of an anisotropic phase (Fig. 7.34A). The lamellar lattice was further confirmed by freeze-fracture transmission electron microscopic and X-ray scattering profiles. Images of uniform parallel lines were obtained from the vitrified sample which showed similar pattern to typical lamellar structures (Fig. 7.34B, C). Further, small and wide angle X-ray scattering evaluations confirmed channel type crystalline bilayers associated in head to head pattern stabilized by strong H-bonding networks (Fig. 7.34F). Lamellar liquid-crystalline mesophases appeared in one direction while in-plane solid-crystalline orders appeared in other two directions. Such observations are characteristic features of transition phase between liquid crystal and solid.

Upon decreasing the mass concentration to 25–6 wt% of region II, large aggregates corresponding to microtubular structures were observed (Jiang et al. 2010a). Generally, tubular assembly is governed by non-directional hydrophobic interactions resulting in less-ordered soft aggregates. However, microtubes formed by the nonamphiphilic self-assembly of sodium dodecyl sulfate@2β-cyclodextrin with mass concentration of 25–6 wt% was driven by directional and ordered H-bonds instead of hydrophobic interactions. The formed microtubes appeared rigid, monodispersed and highly persistent in molecular dimensions owing to strong H-bond interactions. The microtubes were analyzed by confocal laser scanning microscopy using nile red as fluorescent dye that exhibits partial inclusion in the cavity of β-cyclodextrin (Hazra et al. 2004) (Fig. 7.35A, D). The fluorescent walls with non-fluorescent center of microtubes demonstrate the uniform pattern of hollow tubular structures (Fig. 7.35A, D). Similar pattern was observed in the absence of nile red by confocal laser scanning microscopy and transmission electron microscopy (Fig. 7.35B, C). The mean diameter and length of microtubes were 1.1 μm and

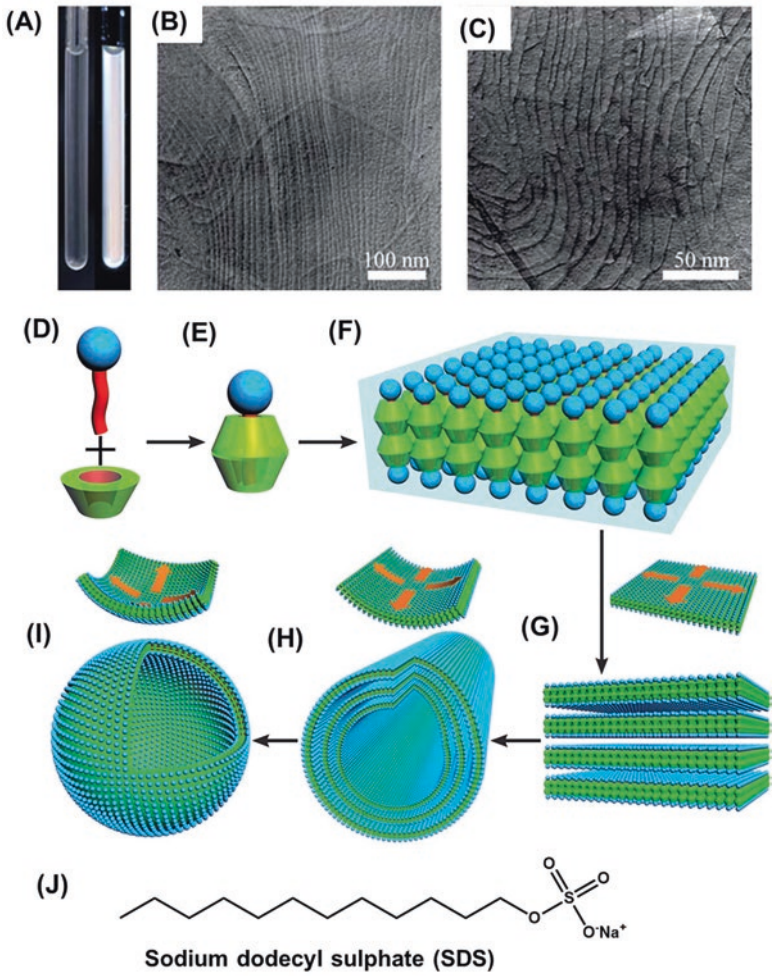

Fig. 7.34 (**A**) NMR sample photographs of 30 wt% sodium dodecyl sulfate@2β-cyclodextrin without (left) and with (right) crossed polarizer. (**B**) and (**C**) freeze-fracture transmission electron micrographs of 30 wt% SDS@2β-cylodextrin complex. (**D–I**) Graphical illustration of sodium dodecyl sulfate@2β- cyclodextrin self-assembly: (**D**) Sodium dodecyl sulfateand *β*-cyclodextrin monomers, (**E**) sodium dodecyl sulfate@2β-cyclodextrin complex, (**F**) Bilayer membrane of sodium dodecyl sulfate@2β- cyclodextrin channels structure. (**G–I**) Transition of lamellae to microtubes and vesicles. (**J**) Structure of sodium dodecyl sulphate (SDS). (**A–I**) are adapted with permission from "(Jiang et al. 2011)". Copyright 2011 Royal Society of Chemistry

40 μm, respectively with wall separation of 0.7 μM. Microtubes appeared quite inflexible as they preferred to be straight rather than bending (Fig. 7.35E). The multilamellar structure of microtubes displayed unique "annular ring" formation, when resolved by freeze-fracture transmission electron microscopy using vitrified sample of sodium dodecyl sulfate@2β-cyclodextrin. Figure 7.35F, H–K illustrates the

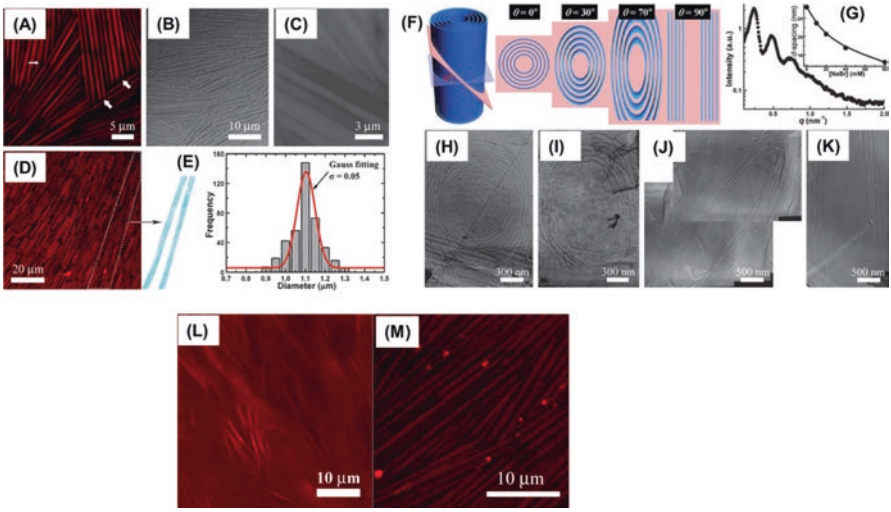

Fig. 7.35 (**A**, **D**) Confocal laser scanning microscopy images of 10 wt% sodium dodecyl sulfate@2β-cyclodextrin solution microtubes, (**B**) Differential interference contrast microscopy image, (**C**) Transmission electron microscopy image, (**E**) Diameter distribution of the microtubes, (**F**–**K**) Annular ring structure of the microtubes. (**F**) Cross sections view of microtube upon changing angle (θ) from 0 to 90° between radical plane and fractured surface, (**G**) Small-angle X-ray scattering profile of the microtubes, and (**H**–**K**) freeze-fracture transmission electron micrography images of the microtubes at different angle (θ) 0° (**H**), 30° (**I**), 70° (**J**), and 90° (**K**). (**A**–**K**) are adapted with permission from (Jiang et al. 2010a). Copyright 2010 Royal Society of Chemistry. (**L** and **M**) are adapted with permission from (Jiang et al. 2010b) and (Jiang et al. 2011). Copyright 2011 Royal Society of Chemistry.

appearance of annular ring changed to circles, ellipses, elongated ellipses and parallel lines upon changing the angle from 0 to 90° between radical plane and fractured surface. Further analysis by atomic-force microscopy and wide-angle X-ray scattering revealed bilayer architecture of microtubes. The nonamphiphilic self-assembly of sodium dodecyl sulfate@2β-cyclodextrin complex to microtubules was attributed to the H-bonding and electrostatic interactions between each complex. Such results were quite interesting since recently, tubular assembled architectures have gained considerable attention in different applications including sensing, synthesis, and drug delivery (Shimizu et al. 2005; Lee et al. 2009).

Structural transformations were also observed upon diluting the mass concentration of sodium dodecyl sulfate@2β-cyclodextrin (6–4%) that led to transition of microtubular to vesicular phases containing unilamellar and bilamellar hollow vesicles with concave/ convex surfaces. Absence of diffraction pattern in small-angle X-ray scattering indicated the formation of unilamellar and bilamellar vesicles instead of multilamellar vesicles. Despite concentration dependency, the recurrent feature of lamellar, microtubular, and vesicle mesophases was the presence of bilayer membrane structures. At the intermediate margins of region I/II and region II/III, concurrence of lamella-microtube for 20 wt% and microtube-vesicle for

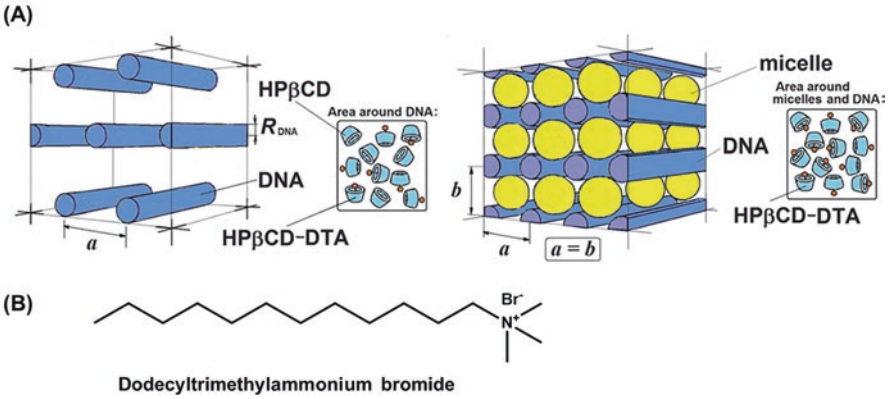

Fig. 7.36 (**A**) Pictorial representation of hexagonal (left) and tetragonal (right) phases of the microstructures of dodecyltrimethylammonium-DNA-(2-Hydroxypropyl)-β-cyclodextrin, respectively. (**B**) Structure of dodecyltrimethylammonium bromide. (**A**) is adapted with permission from (Bilalov et al. 2012). Copyright 2012 Royal Society of Chemistry

7 wt%, respectively were observed using confocal laser scanning microscopy images of entrapped nile red (Fig. 7.35L, M). Figure 7.35L illustrates non-fluorescent center corresponding to hollow microtubes with fluorescent walls of parallel lines as lamellar pattern. Similarly, spherical vesicles were found in the matrix of microtubes validating the cohabitation of lamellae, microtubes and vesicles (Fig. 7.35M). Such nonamphiphilic self-assembly driven by H-bonds and electrostatic interactions instead of hydrophobic interactions promoted the development of new designs to explore self-assembly behavior of cyclodextrin-based liquid crystalline systems.

The lyotropic liquid crystal properties of polyelectrolyte such as deoxyribonucleic acid (DNA) in the biological system depends upon its dispersion in lipids and interaction with counter ions (Dias and Lindman 2008). To this account, the aggregation of polyelectrolytes (DNA) and amphiphilic counter ions dodecyltrimethylammonium was investigated in the absence as well as in the presence of *β*-cylclodextrin and (2-hydroxypropyl)-β-cyclodextrin (Bilalov et al. 2012). In aqueous medium, DNA and dodecyltrimethylammonium essentially form self-assembled water-insoluble micelles and consequently change the liquid crystal phases of DNA. However, the presence of β-cyclodextrin or (2-hydroxypropyl)-β-cyclodextrin, as dispersion agents, redefines the liquid crystalline ordering of DNA by forming inclusion complexes with dodecyltrimethylammonium. The resulted amphiphiles are characterized by a greater degree of dispersion and increased solubility in water. With molar ratio R < 1 (R = [dodecyltrimethylammonium]/[cyclodextrin]) and increased dodecyltrimethylammonium-DNA concentration, 2D hexagonal liquid crystalline phases were observed (Fig. 7.36A, left). Upon further increasing the R > 1.5–2 and dodecyltrimethylammonium-DNA concentration, anisotropic tetragonal liquid crystal lattice possessing square packing was obtained

(Fig. 7.36A, right). Interestingly, both 2D-tetragonal and 2D-hexagonal phases displayed parallel ordering of DNA duplexes.

The rigidity of polyelectrolyte dictates its phase behavior in aqueous medium, hence lyotropic liquid crystal properties. To validate the rigidity effect, a flexible electrolyte, polyacrylate was investigated and compared with DNA, which is relatively rigid (Carlstedt et al. 2012). An isotropic phase was observed in dodecyltrimethylammonium– polyacrylate with molar ratio R = 1 which was similar to dodecyltrimethylammonium–DNA system. With 20 weight percent of (2-hydroxypropyl)-β-cyclodextrin and R ≈ 2, dodecyltrimethylammonium–polyacrylate demonstrated optically isotropic and viscous cubic phase which was further validated by singlet in ^{2}H-NMR spectra. Under similar composition of 20 wt %, hexagonal phase was also observable as optically anisotropic, and viscous with quadrupolar splitting pattern in ^{2}H-NMR spectra. The cubic phase order of dodecyltrimethylammonium–polyacrylate system, and hexagonal and tetragonal phases of dodecyltrimethylammonium–DNA system were attributed to flexible nature of polyacrylate and stiffness of DNA, respectively while keeping the *β*-cyclodextrin and (2-hydroxypropyl)-β-cyclodextrin as the dispersion agents.

7.4 Applications of Cyclodextrin Based Liquid Crystals

7.4.1 Biosensing Based Inclusion and Cholesterol Detection

Over the years, liquid crystals have been used in numerous applications owing to their optical and dielectric anisotropic properties. These include liquid crystal displays, (Hee Lee et al. 2012; Bremer et al. 2013) technical (Goossens et al. 2016) and biological areas (Brake et al. 2003a; Mushenheim et al. 2014). Exploring the liquid crystal behavior at the interface of immiscible phases gave valuable insight on the self-assembled interactions of biomolecules such as proteins (Brake and Abbott 2002) and lipids (Hartono et al. 2008), as well as synthetic molecules including polymers (Brake et al. 2003b) and surfactants (Bai and Abbott 2011).

At the interface, the specific orientational order of liquid crystals changes into different order in presence of interfacial events. These transitions have been successfully applied as imaging tool for the investigating the biomolecular interactions at the cellular level (Park and Abbott 2008; Bi et al. 2009; Lowe and Abbott 2012). Zuo et al. (2014) used this strategy to investigate the host-guest interactions between β-cyclodextrin and sodium dodecylsulfate as well as methylene blue by employing a known mesogen, 4-cyano-4′-pentylbiphenyl (5CB), as nematic liquid crystals analyzed by cross-polarized optical microscopy. At aqueous interface, 4-cyano-4′-pentylbiphenyl self-assemble into nematic liquid crystals with bright images indicating their planer orientations (Fig. 7.37A). With addition of sodium dodecylsulfate, its hydrophobic tail was observed to interact with 4-cyano-4′-pentylbiphenyl that changed their orientations from planer to homeotropic, resulting in dark images of liquid crystals (Fig. 7.37A, B). Further, with the introduction of β-cyclodextrin, the

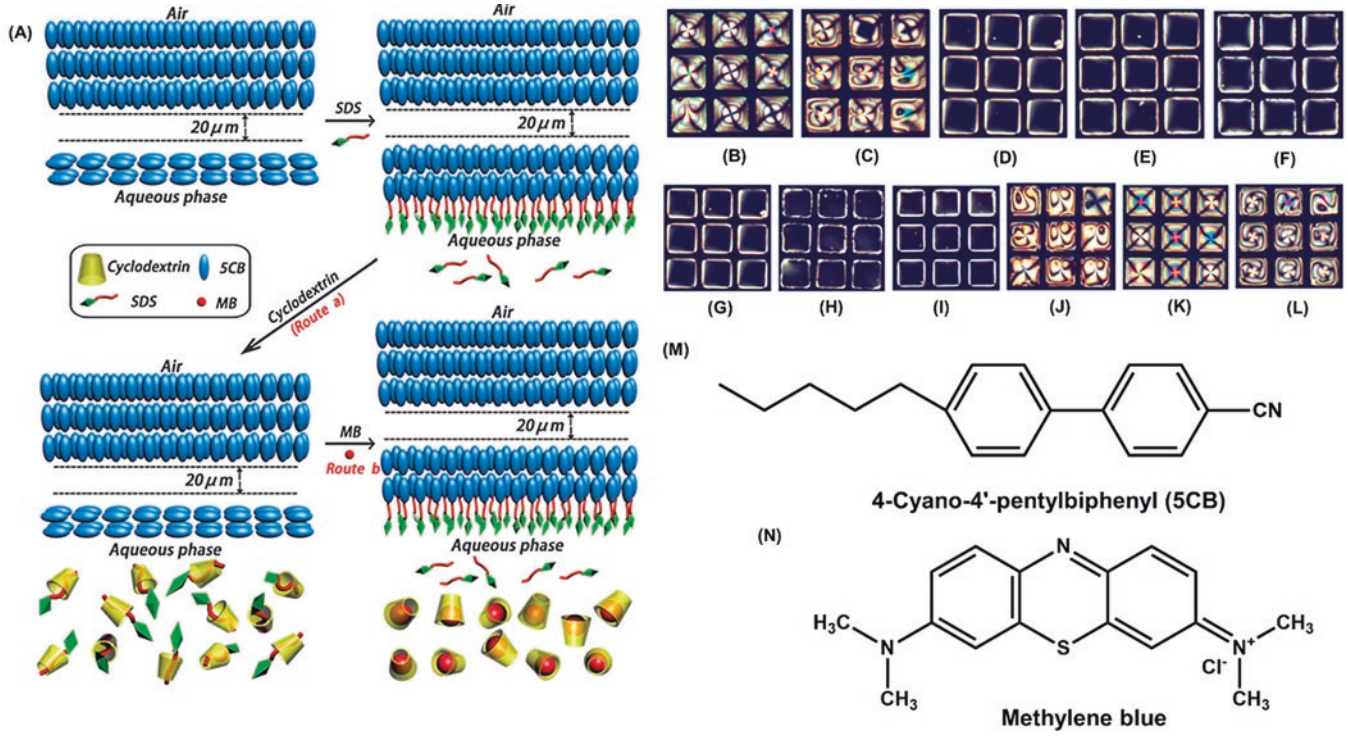

Fig. 7.37 (**A**) Graphical illustration of host–guest complexation between β-cyclodextrin and sodium dodecylsulfate (or methylene blue) using a 4-cyano-4′-pentylbiphenyl LC sensor. (**B**-**F**) Cross-polarized images of copper grid containing 4-cyano-4′-pentylbiphenyl upon addition of various concentrations of sodium dodecylsulfate (mM): (**B**) 0, (**C**) 0.1, (**D**) 0.25, (**E**) 1.0, (**F**) 2.5. (**G**-**L**) Cross-polarized images of copper grid containing 5CB-SDS after addition of various concentrations of β-cyclodextrin (mM): (**G**) 0, (**H**) 0.1, (**I**) 0.25, (**J**) 0.8, (**K**) 1.0, (**L**) 2.5, concentration of sodium dodecylsulfate used = 0.25 mM. (**M** and **N**) Structure of 4-cyano-4′pentylbiphenyl (5CB) and methylene blue (**A**-**L**) are adapted with permission from (Zuo et al. 2014). Copyright 2013 Royal Society of Chemistry

sodium dodecylsulfate molecules showed better inclusion binding with β-cyclodextrin cavity leaving 4-cyano-4′-pentylbiphenyl to reorients themselves from homeotropic to planer order (Fig. 7.37A, C). This resulted into the reappearance of bright images (Fig. 7.37C). No significant change in optical appearance of 4-cyano-4′-pentylbiphenyl was observed upon addition of β-cyclodextrin in the absence of sodium dodecylsulfate except minor color change attributed to weaker 4-cyano-4′-pentylbiphenyl and β-cyclodextrin interactions. To validate the host-guest inclusion interactions, they employed methylene blue that exhibit stronger binding to β-cyclodextrin than sodium dodecylsulfate. Upon exposure of methylene blue to the interfacial solution of 4-cyano-4′-pentylbiphenyl +β-cyclodextrin+sodium dodecylsulfate on the copper grid, the dark images corresponding to homeotropic order reappeared after 30 mins. This is due to the greater binding affinity of methylene blue for the β-cyclodextrin cavity, resulting in the expulsion sodium dodecylsulfate molecules which interact with 4-cyano-4′-pentylbiphenyl again to form dark images.

The LC behavior of ternary complex 4-cyano-4′-pentylbiphenyl + β-cyclodextrin+sodium dodecylsulfatein the presence of methylene blue and dopamine was further investigated by quantum mechanical calculations using Gaussian 09 program package (Liu et al. 2016). PM3 semi-empirical method was used to simulate inclusion complexes of 4-cyano-4′-pentylbiphenyl, β-cyclodextrin, sodium dodecylsulfate, methylene blue, and dopamine which were again re-augmented at DFT B3LYP/6-31G(d) level. The theoretical analysis revealed that sodium dodecylsulfate formed strong inclusion complex with β-cyclodextrin at the interface of 4-cyano-4′-pentylbiphenyl/aqueous surface which resulted in the planer reorientation of liquid crystals. The addition of methylene blue excludes sodium dodecylsulfate from the cyclodextrin cavity to allow the formation of a stronger β-cyclodextrin-methylene blue complex. The simulated energy and complexation profile corroborated 1:2 (methylene blue:2β-cyclodextrin) complex formation through the wider secondary face of cyclodextrin which was more stabilized than sodium dodecylsulfate complex. In addition, it was observed that inclusion complex of dopamine+β-cyclodextrin was less stable than sodium dodecylsulfate+β-cyclodextrin or methylene blue+β-cyclodextrin, therefore no significant change in 4-cyano-4′-pentylbipheyl liquid crystal orientation was found upon addition of dopamine. The theoretical results were in compliance with experimental results observed by Zuo et al.

The inclusion interactions were further extended to examine the specific binding of guest molecule with appropriate host molecule using 4-cyano-4′-pentylbipheyl as liquid crystal imaging tool (Liao et al. 2015). α-cyclodextrin and β-cyclodextrin inherit different cavity sizes, thereby exhibiting different binding affinity for guest molecules. To validate this, they used cetyltrimethyl ammonium bromide as surfactant which exhibits different binding abilities toward α-cyclodextrin and β-cyclodextrin. The orientational order and optical appearance of 4-cyano-4′-pentylbiphenyl in the presence of cetyltrimethyl ammonium bromide was similar to sodium dodecylsulfate pattern. In the presence of cetyltrimethyl ammonium bro-

mide, the planer orientation and bright images of copper grid coated with 4-cyano-4′-pentylbiphenyl changed to homeotropic order and its characteristic dark images. The reverse effect, regeneration of bright images and planer order, was observed upon exposure of 4-cyano-4′-pentylbiphenyl + cetyltrimethyl ammonium bromide films to α-cyclodextrin and β-cyclodextrin solutions. Interestingly, the rate of that transition was much faster for α-cyclodextrin than β-cyclodextrin. It was observed that, at the same concentration and time interval, the cetyltrimethyl ammonium bromide exhibited stronger affinity towards α-cyclodextrin and β-cyclodextrin as visualized by cross-polarized optical microscopy images, surface tension analysis and isothermal titration curve.

For the practical utility of this approach, competitive host-guest interactions at the liquid crystal-aqueous phases have been exploited for the detection of cholesterol and cholic acid. Cholesterol is a valuable component of cell membrane (Ikonen 2008) involved substantially in the biosynthesis of vitamin D and bile acids (Ram et al. 2001a). The high cholesterol level in the blood is implicated in cardiovascular and other diseases by plaque formation in the arteries. Thus, cholesterol detection by simple and effective method is always desirable despite currently available methods including electrochemical, (Dey and Raj 2010) enzyme-based biosensors, (Devadoss and Burgess 2002) and fluorescence spectroscopy (Mondal and Jana 2012). Park et al. developed a cholesterol biosensor by utilizing the sodium dodecyl sulfate/β-cyclodextrin complex on the interface of liquid crystal and aqueous medium (Munir and Park 2015). At the interface between aqueous medium and nematic liquid crystal, the small perturbation can make diverse changes in the orientation of nematic liquid crystal. Such behavior was utilized for cholesterol detection. Sodium dodecyl sulfate forms inclusion complex with β-cyclodextrin owing to host guest interactions (*vide supra*, Fig. 7.37A). The exposure of cholesterol at the interface between aqueous solution and nematic liquid crystal excludes the sodium dodecyl sulfate from sodium dodecyl sulfate/β-cyclodextrin complex due to stronger inclusion of cholesterol into β-cyclodextrin cavity. The excluded sodium dodecyl sulfate gets adsorbed at the interface, thereby changed the orientation of 4-cyano-4′-pentylbiphenyl as demonstrated by cross-polarized optical microscopy. The inclusion concentration of sodium dodecyl sulfate (340 μM) in sodium dodecyl sulfate/β-cyclodextrin complex was carefully analyzed using pH and high-performance liquid chromatography studies. The polarized optical microscope images of 4-cyano-4′-pentylbiphenyl anchored transmission electron microscopy grid cells showed in-plane birefringence illustrating their planer orientation at the interface. Similar planer orientations and bright coloring of cross-polarized optical microscope images were observed in the absence of cholesterol. The addition of cholesterol solution of varying concentrations changed the orientation of 4′-pentylbiphenyl from planer to homeotropic with appearance of dark patches attributed to exclusion of sodium dodecyl sulfate from sodium dodecyl sulfate/β-cyclodextrin complex. The calculated detection limit of cholesterol using this method was 3 μM which is biological relevant detection concentration. The insensitive liquid crystal behavior of 4-cyano-4′-pentylbiphenyl to common interfering analytes present in blood

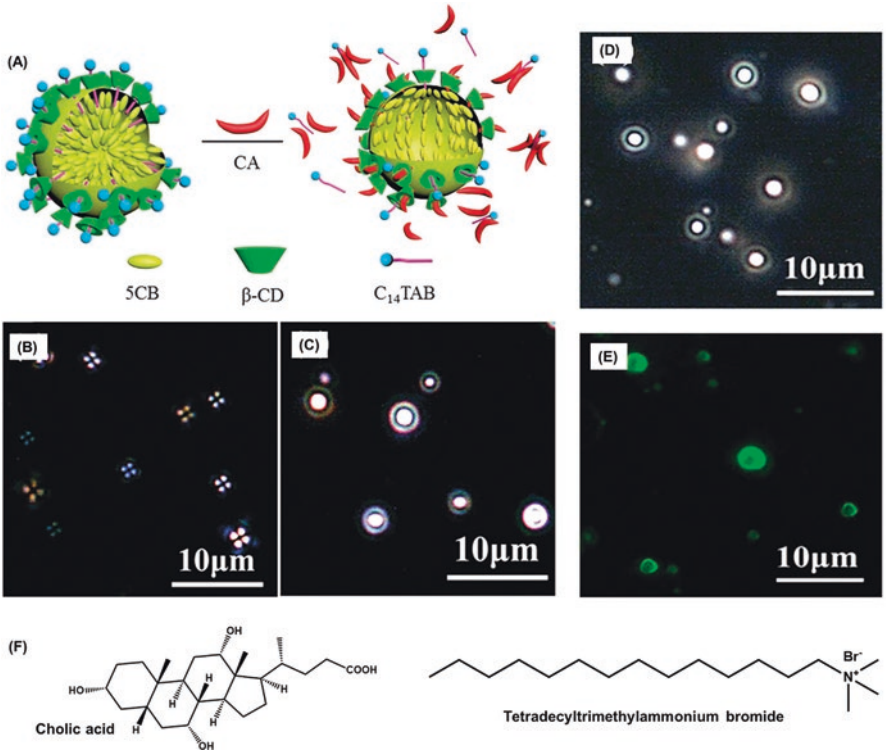

Fig. 7.38 (**A**) Pictorial representation of cholic acid-induced transition of 4-cyano-4′-pentylbiphenyl-β-cyclodextrin-C_{14}TAB(5CB-β-CD-C_{14}TAB) droplets from radial-to-bipolar configuration host–guest recognition. (**B**, **C**) Polarized optical microscope images of 4-cyano-4′-pentylbiphenyl-β-cyclodextrin-C_{14}TAB droplets before (**B**) and after (**C**) addition of 20 mM cholic acid at pH 7.4. (**D**, **E**) Polarized (**D**) and fluorescence (**E**) images of 4-cyano-4′-pentylbiphenyl-β-cyclodextrin-C_{14}TAB droplets after addition of cholyl-lysyl-fluorescein, a fluorescent cholic acid. (**F**) Structure of cholic acid and tetradecyltrimethylammonium bromide. (**A**–**E**) are adapted with permission from (Deng et al. 2015). Copyright 2015 Royal Society of Chemistry

including sodium chloride, hemoglobin, ascorbic acid, and glucose validated the practical utility of this method.

The liquid crystal-aqueous interface self-assembled system was also used to detect cholic acid, a primary component (31%) of bile acids excreted by liver (Hofmann and Hagey 2008). The abnormal production of cholic acid directly correlates with the progress of liver disease (Rani et al. 2004). The concentration analysis of cholic acid in serum and urine provides valuable diagnosis of liver disease and associated treatment (Jorquera et al. 2005; Griffiths and Sjövall 2010). Fang et al. used β-cyclodextrin-C_{14}TAB (tetradecyl trimethylammonium bromide) complex appended 4-cyano-4′-pentylbiphenyl droplets for the facile detection of cholic acid (Fig. 7.38) (Deng et al. 2015). C_{14}TAB formed 1:1 complex with β-cyclodextrin in aqueous system with hydrophilic head and hydrophobic tail oriented toward

secondary and primary faces, respectively (Valente and Söderman 2014). The primary face of β-cyclodextrin-C_{14}TAB complex partially protrudes hydrophobic tail (about 13 Å) which procures this complex a supramolecular surfactant behavior, allowing interactions with 4-cyano-4′-pentylbiphenyl liquid crystals. Cross-polarized optical images and positive zeta potential (+17.6 mV) of β-cyclodextrin-C_{14}TAB-appended-4-cyano-4′-pentylbiphenyl films illustrated the formation of radial configuration in which primary and secondary faces of β-cyclodextrin were oriented toward 4-cyano-4′-pentylbiphenyl and water phases, respectively. The addition of cholic acid changed the radial configuration of β-cyclodextrin-C_{14}TAB-appended-4-cyano-4′-pentylbiphenyl films to bipolar configuration (Fig. 7.38B, C) attributed to the inclusion of cholic acid into cavity of β-cyclodextrin through its primary face and consequently exclusion of C_{14}TAB. This was validated by observing decrease in surface tensions of 20 μM CA solution (52.6 mN m^{-1} for) compared to 1.6 mM solution of β-cyclodextrin-C_{14}TAB (54.8 mN m^{-1}) suggesting 27.5% displacement of C_{14}TAB. The complexation of cholic acid with β-cyclodextrin-C_{14}TAB-appended-4-cyano-4′-pentylbiphenyl films was further verified by their bipolar fluorescent images measured by confocal microscope using cholyl-lysyl-fluorescein, a fluorescence derivative of cholic acid (Fig. 7.38D, E). The detection limit of the cholic acid was found to be 20 μM using liquid crystal imaging method. Furthermore, cholic acid was detected (detection limit = 60 μM) in synthetic urine sample (3.16 mM urea, 42.6 μM $MgSO_4$, 90.1 μM $CaCl_2$, and 1.36 mM NaCl) in the presence of interfering uric acid and urea, validating the practical utility of this method. Similar liquid crystalline behavior of 4-cyano-4′-pentylbiphenyl was observed upon interaction with (2-hydroxylpropyl)-β-cyclodextrin-C_{16}TAB complex highlighting the uniformity of detection method.

7.4.2 CD Capped Nanoparticle and Liquid Crystal Displays

From last few decades, utilization of liquid crystal displays (LCD) and their electro-optic properties have flourished significantly in the electronic and communication industries. Despite their huge utility in revolutionizing modern technology, liquid crystal displays have been associated with slow electro-optical response. Various modifications have been done by doping liquid crystals with semiconductor nanoparticles (Du and Toshima 2007), carbon nanotubes (Chen and Lee 2006), metal nanoparticles (Shiraishi et al. 2002) and fullerene (Suzuki et al. 2001) to enhance response time and contrast, and lowering the driving voltage of liquid crystal displays. Cyclodextrin-capped SiO_2 nanoparticles (Cyclodextrin = α-cyclodextrin, β-cyclodextrin, γ-cyclodextrin and poly-γ-cyclodextrin) have also been utilized for doping liquid crystals of 4-cyano-4′-pentylbiphenyl to enhance their response time. (Shiraishi et al. 2012). The dispersion of cyclodextrin-SiO_2 into the liquid crystals of 4-cyano-4′-pentylbiphenyl resulted into twisted nematic liquid crystal (TN-LCD) with comparative faster response time than pure 4-cyano-4′-pentylbiphenyl. The capped cyclodextrin-SiO_2 formed homogenous nanoparticles with average diameter

of 9.4, 8.4, 10.6, and 6.4 nm for α-cyclodextrin, β-cyclodextrin, γ-cyclodextrin and poly-γ-cyclodextrin, respectively corresponding to their protecting abilities (β-cyclodextrin > α-cyclodextrin > γ-cyclodextrin) (Komiyama and Hirai 1983). Doping of cyclodextrin-SiO_2 with 4-cyano-4′-pentylbiphenyl liquid crystals resulted in formation of twisted nematic liquid crystal with similar phase transition temperature (4-cyano-4′-pentylbiphenyl = 34.2 °C, α-cyclodextrin = 34.2 °C, β-cyclodextrin = 34.1 °C, and γ-cyclodextrin = 34.1 °C). The response time (τ_{on}: rise time of 90% -10% transmittance, and τ_{off}: fall time of 10%–90% transmittance) of twisted nematic liquid crystal of cyclodextrin-SiO_2 appended 4-cyano-4′-pentylbiphenyl were obtained by measuring the transmission of liquid crystals. Faster response time was observed for twisted nematic liquid crystal of cyclodextrin-SiO_2 + 4-cyano-4′-pentylbiphenyl (76.7, 71.5, and 90.7 msec for α-cyclodextrin, β-cyclodextrin, and γ-cyclodextrin respectively) compared to 96.2 msec of 4-cyano-4′-pentylbiphenyl alone attributed to capping, protection and solubilizing properties of cyclodextrin. Comparatively, β-cyclodextrin-SiO_2 + 4-cyano-4′-pentylbiphenyl liquid crystals showed faster response time over α-cyclodextrin, and γ-cyclodextrin due to better inclusion of 4-cyano-4′-pentylbiphenyl in β-cyclodextrin cavity. To visualize the practical utility of doped system, a liquid crystal device was developed using M03 (a commonly used practical liquid crystal in display industries) as host liquid crystal and poly-γ-cyclodextrin as stabilizer owing to its higher stability for longer time and better fall time. An enhanced response time of poly-γ-cyclodextrin-SiO_2 doped M03 liquid crystal display was observed validating its industrial application.

Further experiments were performed to investigate the doping effect of different metal nanoparticles such as barium titanate ($BaTiO_3$) (Shiraishi et al. 2015) and ZrO_2/Au (Shiraishi et al. 2016) capped with cyclodextrin on liquid crystals performance. Barium titanate exhibits high dielectric constant and ferroelectric properties, explaining its numerous applications such as electro-optical displays, and thermistors. Doping of nematic liquid crystals with $BaTiO_3$ were found to have strong electromechanical polarization fluctuations (Basu 2014) and pretransitional effects on the isotropic to nematic phase transitions (Čopič et al. 2007). To increase the compatibility and response time of liquid crystals, barium titanate was capped with γ-cyclodextrin and mixed with liquid crystals of 4-cyano-4′-pentylbiphenyl. Particles of γ-cyclodextrin appended barium titanate (2.1 nm diameter) prepared using microwave/ ultra-sonication showed better response time compared to solvothermal method (2.3 nm, 2.7 nm and 3.9 nm, at 240 °C, 270 °C and 300 °C, respectively) due to their higher dispersion with liquid crystals of 4-cyano-4′-pentylbiphenyl. Faster response of γ-cyclodextrin- $BaTiO_3$ doped 4-cyano-4′-pentylbiphenyl with τ_{on} = 58.55 msec and τ_{off} = 14.49 msec was found compared to pure 4-cyano-4′-pentylbiphenyl with τ_{on} = 60.57 msec and τ_{off} = 15.45 msec. The field sequential-color (FSC) specific liquid crystal NTN01 was doped with γ-cyclodextrin-$BaTiO_3$ nanoparticles and transmission was recorded. Response time of 3.99% was enhanced for NTN01 at 25 °C in the presence of γ-cyclodextrin-$BaTiO_3$ nanoparticles (τ_{on} = 10.43 msec and τ_{off} = 4.86 msec; τ_{total} = 15.29 msec) compared to

homologous system in absence of γ-cyclodextrin (τ_{on} = 9.82 msec and τ_{off} = 4.86 msec; τ_{total} = 14.68 msec). On decreasing the temperature to 0 °C, 7.44% faster response time was observed. These results illustrated that doping liquid crystals with *γ*-cyclodextrin capped nanoparticles gave an enhanced activity of electro-optical properties yielding better display devices.

Undoubtedly, the use of metal based nanoparticle dopant in liquid crystalline materials produces favorable physicochemical impact on their display properties. Various dopants induce perturbation and polarization of the orientation pattern of liquid crystal materials, thereby, display different electro-optical properties. Among different kinds of dopants, mono- and bimetallic nanoparticles have shown interesting applicability due to their quantum size and higher surface area (Cao et al. 2010; Corain et al. 2011). On comparing both, bimetallic nanoparticles advantageously possess large and diverse surface area for inducing higher catalytic and capping abilities (Wieckowski et al. 2003). To develop such system, poly-γ-cyclodextrin has been used as capping agent for generating ZrO_2/ Au nanoparticles using ultra-sonication and microwave methods (Shiraishi et al. 2016). Different ratios of ZrO_2/Au (1:1, 2:1, 4:1, and 9:1) were used to formulate nanoparticles of different sizes (4.6 nm, 4.0 nm, 3.1 nm, and 3.1 nm, respectively) as demonstrated by dynamic light scattering (DLS) and transmission electron microscopy images. The addition of poly-γ-cyclodextrin-ZrO_2/Au dopant to NTN01 resulted in transition of isotropic phase to twisted nematic phase. Response times of twisted nematic liquid crystals obtained by mixing poly-γ-cyclodextrin-ZrO_2/Au and NTN01 were evaluated for different ratio of ZrO_2/Au. Compared to pure NTN01, Poly-γ-cyclodextrin-ZrO_2/Au doped twisted nematic liquid crystal exhibited enhanced response time, illustrating the structural diversity effect of poly-γ-cyclodextrin and ZrO_2/Au particles on liquid crystalline behavior. Further, improved response rate was observed for ZrO_2/Au (4:1) ratio compared to lower ratios of ZrO_2/Au (2:1) and ZrO_2/Au (1:1) ratios. Thus, developing better liquid crystal displays by doping available liquid crystals with different dopants would be an advantageous strategy for reducing ill effects of modern technologies.

7.4.3 Discrete Applications

Using a combination strategy of cyclodextrin and liquid crystals, the discrimination of enantiomers discrimination has been reported. Normally, NMR spectroscopy is the technique used to discriminate enantiomers with the help of a chiral auxiliary, by taking advantage of the diastereomeric interaction between the added chiral auxiliary and each enantiomer. In order to observe appreciable chemical shifts, strong diastereomeric interactions are required. An alternative method was developed to discriminate enantiomers using cyclodextrin (β-cyclodextrin and (2-hydroxypropyl)-β-cyclodextrin) as chiral cages in non-chiral liquid crystal solvent (Péchiné et al. 2002). The different inclusion and orientation of enantiomers in chiral cages

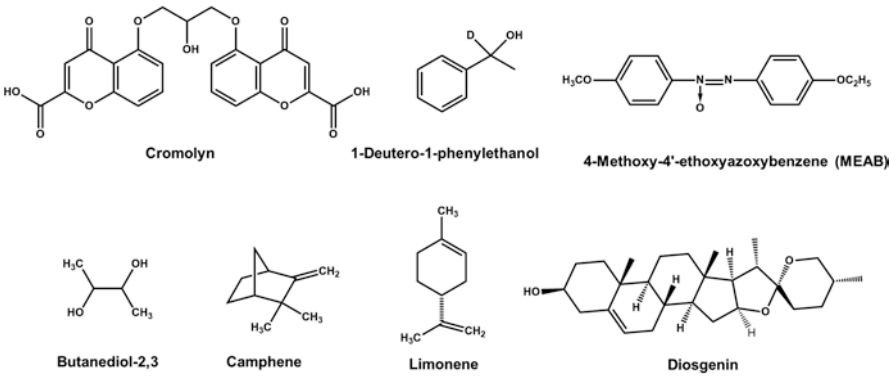

Fig. 7.39 Structures of different compounds used in various studies

produce significant and easily observable chemical shifts in the NMR spectra. Cromolyn was used as nematic liquid crystal phase in water and 1-deutero-1-phenylethanol was used as chiral compound with racemic and (S)-enriched species (Fig. 7.39). The NMR spectrum of racemic mixture showed 3 deuterium quadrupolar splittings when dissolved in cromolyn-β-cyclodextrin mesophase. Two inner doublets corresponding to encaged enantiomers with quadrupolar splittings were observe; the outer doublets correspond to outside cavity enantiomers. Thus, the different orientation of the encaged enantiomer in β-cyclodextrin cavity in liquid crystal phase allowed their differentiation.

In another application, chiral nematic liquid crystals with helically twisted mesophase were obtained as chiral sorbent, by mixing the achiral nematic liquid crystals of 4-methoxy-4′-ethoxyazoxybenzene (MEAB) with acetyl-β-cyclodextrin as chiral auxiliary (Fig. 7.39) (Onuchak et al. 2012). Higher melting enthalpy of sorbent by 2.57% compared to 4-methoxy-4′-ethoxyazoxybenzene was observed, confirming intermolecular interactions between them in twisted mesophase. The sorption properties, including separation and thermodynamic functions of these chiral sorbent, were investigated toward different organic molecules including alkanes, cycloalkanes, camphene, limonene alcohols, heterocycles, butanediol-2,3 and aromatic molecules (Fig. 7.39). The structural and enantiomeric selectivity of investigated molecules depend upon the transition temperature range of sorbent, i.e. 95–120 °C for structural and 91–100 °C for enantiomeric, respectively. The polar and aromatic sorbates showed positive sorption contributions (δ) owing to their host guest interactions with acetyl-β-cyclodextrin. However, negative sorption contributions for other sorbates were observed, due to highly ordered structure and solvation effect between liquid crystal-cyclodextrin that hindered their interactions. Further, (+) isomers of butanediol-2,3, camphene, and limonene showed better enantioselectivity compared to (−) isomers due to a better compatibility with the D-(+)-glucopyranose units of acetyl-β-cyclodextrin in temperature window of 91–100 °C.

For biological applications, cyclodextrin are among the most suitable scaffolds owing to their biocompatibility and low cytotoxicity profile. Diosgenin (Fig. 7.39), (Final Report of the Amended Safety Assessment of Dioscorea Villosa (Wild Yam) Root Extract, 2004) a steroidal saponin, is a multifunctional molecule with numerous applications including plasma glucose (Pari et al. 2012) and cholesterol inhibitor (Gong et al. 2010), source of steroid hormones, dietary supplement and melanogenesis inhibitor (Lee et al. 2007). The bioavailability of diosgenin for medical applications is very limited due to its poor aqueous solubility; however, upon complexation with β-cyclodextrin, its solubility improves significantly. Okawara et al. (2014) used a combination of diosgenin, liquid crystalline amphipathic lipids: glyceryl monooleate and phytantriol and β-cyclodextrin, to investigate their enhanced solubility profile. Glyceryl monooleate and phytantriol exhibited self-assembled and dispersed liquid crystalline properties. The small-angle X-ray scattering analysis of glyceryl monooleate-diosgenin and phytantriol-diosgenin mixtures confirmed the formation of hexagonal and cubic mesophases of 100 and 200 nm respectively. The solubility and plasma concentration of diosgenin significantly increased upon mixing with glyceryl monooleate or phytantriol lipids illustrating enhanced permeation across intestinal mucosa. Comparatively, these effects are better for glyceryl monooleate than phytantriol, which were further enhanced upon addition of β-cyclodextrin. Pharmacokinetic analysis of oral administration of glyceryl monooleate-diosgenin- β-cyclodextrin and phytantriol-diosgenin-β-cyclodextrin to Wistar rats revealed higher diosgenin distribution across skin compared to diosgenin suspension alone with minimal undesired toxicity. Thus, these results validated the benefit of using β-cyclodextrin to enhance the drug solubility and bioavailability, resulting in better pharmacokinetics.

7.5 Conclusion

Since the first report of cyclodextrin-based thermotropic liquid crystals, over the years, several families of cyclodextrin-based liquid crystal materials have been reported. However, comparing to other types of materials, the research in developing cyclodextrin-based liquid crystal materials has been relatively slow. Overall, the design of self-assembled cyclodextrin materials can take advantages of fundamental intermolecular forces such as H-bonding, dipole-dipole interactions, as well as π-π interactions. Interestingly, the use of weaker interaction forces appears to generate materials with improved fluidity and richer phase transitions. Although native cyclodextrin molecules are incapable of forming thermotropic liquid crystals, the introduction of mesogenic groups can produce various mesophases such as nematic, smectic, and columnar. Photoresponsive systems were also obtained by conjugating azobenzene moieties to cyclodextrin scaffolds. Several polymeric liquid crystalline materials were demonstrated which possess very interesting properties. Even after all these investigations, several unanswered questions remain. More investigations are needed to tune the materials in order to be commercially viable.

Acknowledgements The financial support from Alberta Innovates – Technology Futures, the Natural Sciences and Engineering Research Council of Canada, and the University of Calgary are greatly acknowledged.

References

Araki J, Sato H, Takagi Y, Ohta K (2014) "Molecular rope curtain" type of liquid crystals based on a sliding graft copolymer having mobile peg side chains. Mol Cryst Liq Cryst 592:99–105. https://doi.org/10.1080/07315171.2013.840758

Ashton PR, Ellwood P, Staton I, Stoddart JF (1991) Per-3,6-anhydro-alpha-cyclodextrin and per-3,6-anhydro-beta-cyclodextrin. J Org Chem 56:7274–7280. https://doi.org/10.1021/jo00026a017

Ashton PR, Boyd SE, Gattuso G, Hartwell EY, Koeniger R, Spencer N et al (1995) A novel approach to the synthesis of some chemically-modified cyclodextrins. J Org Chem 60:3898–3903. https://doi.org/10.1021/jo00117a049

Avakyan VG, Nazarov VB, Alfimov MV, Bagatur AA, Voronezheva NI et al (2001) The role of intra-and intermolecular hydrogen bonds in the formation of β-cyclodextrin head-to-head and head-to-tail dimers. The results of ab initio and semiempirical quantum-chemical calculations. Russ Chem Bull 50:206–216. https://doi.org/10.1023/A:1009557729668

Ba C-Y, Shen Z-R, Gu H-W, Guo G-Q, Xie P, Zhang R-B et al (2003) A triphenylene-containing side chain liquid crystalline ladder-like polysiloxane and its highly ordered superstructure. Liq Cryst 30:391–397. https://doi.org/10.1080/0267829031000089924

Bai Y, Abbott NL (2011) Recent advances in colloidal and interfacial phenomena involving liquid crystals. Langmuir 27:5719–5738. https://doi.org/10.1021/la103301d

Barnes WH, Ross S (1936) The diffraction of X-rays by the higher polyethylene glycols and by polymerized ethylene oxides1. J Am Chem Soc 58:1129–1131. https://doi.org/10.1021/ja01298a018

Basu R (2014) Soft memory in a ferroelectric nanoparticle-doped liquid crystal. Phys Rev E 89:022508. https://doi.org/10.1103/PhysRevE.89.022508

Bi X, Hartono D, Yang K-L (2009) Real-time liquid crystal pH sensor for monitoring enzymatic activities of penicillinase. Adv Funct Mater 19:3760–3765. https://doi.org/10.1002/adfm.200900823

Bilalov A, Carlstedt J, Krivtsova E, Lindman B, Olsson U (2012) DNA with amphiphilic counterions: tuning colloidal DNA with cyclodextrin. Soft Matter 8:4988. https://doi.org/10.1039/c2sm25058f

Bonini M, Rossi S, Karlsson G, Almgren M, Lo Nostro P, Baglioni P (2006) Self-assembly of β-cyclodextrin in water. Part 1: Cryo-TEM and dynamic and static light scattering. Langmuir 22:1478–1484. https://doi.org/10.1021/la052878f

Bortel E, Hodorowicz S, Lamot R (1979) Relation between crystallinity degree and stability in solid state of high molecular weight poly(ethylene oxide)s. Macromol Chem Phys 180:2491–2498. https://doi.org/10.1002/macp.1979.021801023

Bouteiller L, Barny PL (1996) Polymer-dispersed liquid crystals: preparation, operation and application. Liq Cryst 21:157–174. https://doi.org/10.1080/02678299608032820

Brake JM, Abbott NL (2002) An experimental system for imaging the reversible adsorption of amphiphiles at aqueous−liquid crystal interfaces. Langmuir 18:6101–6109. https://doi.org/10.1021/la011746t

Brake JM, Daschner MK, Luk Y-Y, Abbott NL (2003a) Biomolecular interactions at phospholipid-decorated surfaces of liquid crystals. Science 302:2094–2097. https://doi.org/10.1126/science.1091749

Brake JM, Mezera AD, Abbott NL (2003b) Active control of the anchoring of 4‘-pentyl-4-cyanobiphenyl (5CB) at an aqueous−liquid crystal interface by using a redox-active ferrocenyl surfactant. Langmuir 19:8629–8637. https://doi.org/10.1021/la034469u

Bremer M, Kirsch P, Klasen-Memmer M, Tarumi K (2013) The TV in your pocket: development of liquid-crystal materials for the new millennium. Angew Chem Int Ed 52:8880–8896. https://doi.org/10.1002/anie.201300903

Cammidge AN, Gopee H (2009) Synthesis and liquid crystal properties of mixed alkynyl-alkoxytriphenylenes. Liq Cryst 36:809–816. https://doi.org/10.1080/02678290903063000

Cao A, Lu R, Veser G (2010) Stabilizing metal nanoparticles for heterogeneous catalysis. Phys Chem Chem Phys 12:13499–13510. https://doi.org/10.1039/C0CP00729C

Carlstedt J, Bilalov A, Olsson U (2012) Aqueous phase behavior of polyelectrolytes with amphiphilic counterions modulated by cyclodextrin: the role of polyion flexibility. Phys Chem Chem Phys 14:9574. https://doi.org/10.1039/c2cp41353a

Challa R, Ahuja A, Ali J, Khar RK (2005) Cyclodextrins in drug delivery: an updated review. AAPS PharmSciTech 6:E329–E357. https://doi.org/10.1208/pt060243

Champagne P-L, Ester D, Ward S, Williams V E, Ling C-C (2016) A family of amphiphilic cyclodextrin liquid crystals governed by dipole–dipole interactions. ChemPlusChem n/a-n/a doi:https://doi.org/10.1002/cplu.201600556

Chen H-Y, Lee W (2006) Suppression of field screening in nematic liquid crystals by carbon nanotubes. Appl Phys Lett 88:222105. https://doi.org/10.1063/1.2208373

Chen L, Hu T-H, Xie H-L, Zhang H-L (2010) A mixed cyclodextrin-biphenyl thermotropic liquid crystal: synthesis, liquid-crystalline properties, and supramolecular organization. J Polym Sci A Polym Chem 48:2838–2845. https://doi.org/10.1002/pola.24060

Collings PJ, Hird M (1997) Introduction to liquid crystals: chemistry and physics. CRC Press

Čopič M, Mertelj A, Buchnev O, Reznikov Y (2007) Coupled director and polarization fluctuations in suspensions of ferroelectric nanoparticles in nematic liquid crystals. Phys Rev E 76:011702. https://doi.org/10.1103/PhysRevE.76.011702

Corain B, Schmid G, Toshima N (2011) Metal nanoclusters in catalysis and materials science: the issue of size control. Elsevier

Corruccini RJ, Gilbert EC (1939) The heat of combustion of cis-and trans-azobenzene. J Am Chem Soc 61:2925–2927

Cramer F, Mackensen G, Sensse K (1969) On ring compounds. XX. ORD-spectra and conformation of the glucose ring in cyclodextrins. Chem Ber 102:494–508. https://doi.org/10.1002/cber.19691020217

Cromwell WC, Bystrom K, Eftink MR (1985) Cyclodextrin-adamantanecarboxylate inclusion complexes: studies of the variation in cavity size. J Phys Chem 89:326–332. https://doi.org/10.1021/j100248a029

Davis ME, Brewster ME (2004) Cyclodextrin-based pharmaceutics: past, present and future. Nat Rev Drug Discov 3:1023–1035

Deng J, Lu X, Constant C, Dogariu A, Fang J (2015) Design of β-CD–surfactant complex-coated liquid crystal droplets for the detection of cholic acid via competitive host–guest recognition. Chem Commun 51:8912–8915. https://doi.org/10.1039/C5CC01561H

Devadoss A, Burgess JD (2002) Detection of cholesterol through electron transfer to cholesterol oxidase in electrode-supported lipid bilayer membranes. Langmuir 18:9617–9621. https://doi.org/10.1021/la0258594

Dey RS, Raj CR (2010) Development of an amperometric cholesterol biosensor based on graphene−pt nanoparticle hybrid material. J Phys Chem C 114:21427–21433. https://doi.org/10.1021/jp105895a

Dias R, Lindman B (2008) DNA interactions with polymers and surfactants. Wiley, Hoboken

Doane JW, Vaz NA, Wu B-G, Žumer S (1986) Field controlled light scattering from nematic microdroplets. Appl Phys Lett 48:269–271. https://doi.org/10.1063/1.96577

Dong Y, Lam JW, Peng H, Cheuk KK, Kwok HS, Tang BZ (2004) Syntheses and mesomorphic and luminescent properties of disubstituted polyacetylenes bearing biphenyl pendants. Macromolecules 37:6408–6417. https://doi.org/10.1021/ma049094d

Dorrego AB, García-Río L, Hervés P, Leis JR, Mejuto JC, Pérez-Juste J (2000) Micellization versus cyclodextrin–surfactant complexation. Angew Chem Int Ed 39:2945–2948. doi:10.1002/1521-3773(20000818)39:16<2945::AID-ANIE2945>3.0.CO;2-6

Du Y, Toshima N (2007) Low driving voltage of twisted nematic liquid crystal displays doped with CdS nanoparticles. Bull Chem Soc Jpn 80:2446–2450. https://doi.org/10.1246/bcsj.80.2446

Eftink M, Andy M, Bystrom K, Perlmutter H, Kristol D (1989) Cyclodextrin inclusion complexes - studies of the variation in the size. J Am Chem Soc 111:6765–6772. https://doi.org/10.1021/ja00199a041

Fügedi P (1989) Synthesis of heptakis (6-O-tert-butyldimethylsilyl) cyclomaltoheptaose and octakis (6-O-tert-butyldimethylsilyl) cyclomalto-octaose. Carbohydr Res 192:366–369. https://doi.org/10.1016/0008-6215(89)85197-3

Fujita K, Nagamura S, Imoto T (1984) Convenient preparation and effective separation of the C-2 and C-3 tosylates of α-cyclodextrin. Tetrahedron Lett 25:5673–5676. https://doi.org/10.1016/S0040-4039(01)91409-1

Gadelle A, Defaye J (1991) Selective halogenation at primary positions of cyclomaltooligosaccharides and a synthesis of per-3,6-anhydro cyclomaltooligosaccharides. Angew Chem Int Ed EngL 30:78–80. https://doi.org/10.1002/anie.199100781

Gelb RI, Schwartz LM (1989) Complexation of adamantane-ammonium substrates by beta-cyclodextrin and its O-methylated derivatives. J Incl Phenom Mol Recognit Chem 7:537–543. https://doi.org/10.1007/BF01080464

Gibson HW, Bheda MC, Engen PT (1994) Rotaxanes, catenanes, polyrotaxanes, polycatenanes and related materials. Prog Polym Sci 19:843–945. https://doi.org/10.1016/0079-6700(94)90034-5

Gong G, Qin Y, Huang W, Zhou S, Wu X, Yang X et al (2010) Protective effects of diosgenin in the hyperlipidemic rat model and in human vascular endothelial cells against hydrogen peroxide-induced apoptosis. Chem Biol Interact 184:366–375. https://doi.org/10.1016/j.cbi.2010.02.005

Goossens K, Lava K, Bielawski CW, Binnemans K (2016) Ionic liquid crystals: versatile materials. Chem Rev 116:4643–4807. https://doi.org/10.1021/cr400334b

Gray GW (1962) Molecular structure and the properties of liquid crystals. Academic Press Inc, New York

Griffiths WJ, Sjövall J (2010) Bile acids: analysis in biological fluids and tissues. J Lipid Res 51:23–41. https://doi.org/10.1194/jlr.R001941-JLR200

Gulik A, Delacroix H, Wouessidjewe D, Skiba M (1998) Structural properties of several amphiphile cyclodextrins and some related nanospheres. An X-ray scattering and freeze-fracture electron microscopy study. Langmuir 14:1050–1057. https://doi.org/10.1021/la971019r

Gündüz B (2015) Sensing and surface morphological properties of a poly [(9, 9-dioctylfluorenyl-2, 7-diyl)-co-bithiophene] liquid-crystalline polymer for optoelectronic applications. J Appl Polym Sci 132. Available at: http://onlinelibrary.wiley.com/doi/10.1002/app.41659/pdf. Accessed 15 Feb 2017

Guo A, Yan Z, Ye L, Zhang A, Feng Z (2016) The synthesis and characterization of spacer-free liquid crystal polyrotaxane by virtue of the mobility of threaded α-cyclodextrins. Macromol Chem Phys 217:646–653. https://doi.org/10.1002/macp.201500415

Han X, Chai L, Shanks R, Pavel D (2006) Monte Carlo simulations of properties of side-chain liquid-crystal polymers. Polym Int 55:1323–1329. https://doi.org/10.1002/pi.2087

Harada A, Li J, Kamachi M (1992) The molecular necklace: a rotaxane containing many threaded alpha-cyclodextrins. Nature 356:325. https://doi.org/10.1038/356325a0

Harada A, Li J, Kamachi M (1993) Synthesis of a tubular polymer from threaded cyclodextrins. Nature 364:516–518. https://doi.org/10.1038/364516a0

Harries D, Rau DC, Parsegian VA (2005) Solutes probe hydration in specific association of cyclodextrin and adamantane. J Am Chem Soc 127:2184–2190. https://doi.org/10.1021/ja045541t

Hartono D, Bi X, Yang K-L, Yung L-YL (2008) An air-supported liquid crystal system for real-time and label-free characterization of phospholipases and their inhibitors. Adv Funct Mater 18:2938–2945. https://doi.org/10.1002/adfm.200800424

Hazra P, Chakrabarty D, Chakraborty A, Sarkar N (2004) Intramolecular charge transfer and solvation dynamics of Nile Red in the nanocavity of cyclodextrins. Chem Phys Lett 388:150–157. https://doi.org/10.1016/j.cplett.2004.02.078

He T, Hu T, Zhang X, Zhong G, Zhang H (2009) Synthesis and characterization of a novel liquid crystalline star-shaped polymer based on α-CD core via ATRP. J App Polymer Sci 112:2120–2126. https://doi.org/10.1002/app.29657

Hee Lee S, Sarathi Bhattacharyya S, Seok Jin H, Jeong K-U (2012) Devices and materials for high-performance mobile liquid crystal displays. J Mater Chem 22:11893–11903. https://doi.org/10.1039/C2JM30635B

Hiltrop K (1994) Lyotropic liquid crystals. In: Stegemeyer PDH, Behret GSDH, DB-G für PC e.V (Steinkopff) (ed) Liquid crystals topics in physical chemistry, pp 143–171. https://doi.org/10.1007/978-3-662-08393-2_4

Hirayama F, Uekama K (1999) Cyclodextrin-based controlled drug release system. Adv Drug Deliv Rev 36:125–141. https://doi.org/10.1016/S0169-409X(98)00058-1

Hoare TR, Kohane DS (2008) Hydrogels in drug delivery: progress and challenges. Polymer 49:1993–2007. https://doi.org/10.1016/j.polymer.2008.01.027

Hoeben FJM, Jonkheijm P, Meijer EW, Schenning APHJ (2005) About supramolecular assemblies of π-conjugated systems. Chem Rev 105:1491–1546. https://doi.org/10.1021/cr030070z

Hofmann AF, Hagey LR (2008) Bile acids: chemistry, pathochemistry, biology, pathobiology, and therapeutics. Cell Mol Life Sci 65:2461–2483. https://doi.org/10.1007/s00018-008-7568-6

Phases of Liquid Crystals (n.d.) Available at: http://plc.cwru.edu/tutorial/enhanced/files/lc/phase/phase.htm. Accessed 13 Mar 2016

Hu T, Xie H, Chen L, Chen S, Zhang H (2011) Intriguing liquid crystalline behavior of liquid crystalline polyrotaxane containing azobenzene mesogens. Polym Bull 67:937–950

Ikonen E (2008) Cellular cholesterol trafficking and compartmentalization. Nat Rev Mol Cell Biol 9:125–138. https://doi.org/10.1038/nrm2336

Jiang L, Peng Y, Yan Y, Deng M, Wang Y, Huang J (2010a) "Annular Ring" microtubes formed by SDS@2β-CD complexes in aqueous solution. Soft Matter 6:1731. https://doi.org/10.1039/b920608f

Jiang L, Yan Y, Huang J, Yu C, Jin C, Deng M et al (2010b) Selectivity and stoichiometry boosting of β-cyclodextrin in cationic/anionic surfactant systems: when host−guest equilibrium meets biased aggregation equilibrium. J Phys Chem B 114:2165–2174. https://doi.org/10.1021/jp911092y

Jiang L, Peng Y, Yan Y, Huang J (2011) Aqueous self-assembly of SDS@2β-CD complexes: lamellae and vesicles. Soft Matter 7:1726–1731. https://doi.org/10.1039/C0SM00917B

Jorquera F, Monte MJ, Guerra J, Sanchez-Campos S, Merayo JA, Olcóz JL et al (2005) Usefulness of combined measurement of serum bile acids and ferritin as additional prognostic markers to predict failure to reach sustained response to antiviral treatment in chronic hepatitis C. J Gastroenterol Hepatol 20:547–554. https://doi.org/10.1111/j.1440-1746.2005.03725.x

Karaky K, Reynaud S, Billon L, François J, Chreim Y (2005) Organosoluble star polymers from a cyclodextrin core. J Polym Sci A Polym Chem 43:5186–5194. https://doi.org/10.1002/pola.21012

Kato T, Mizoshita N, Kishimoto K (2006) Functional liquid-crystalline assemblies: self-organized soft materials. Angew Chem Int Ed 45:38–68

Katsuno C, Konda A, Urayama K, Takigawa T, Kidowaki M, Ito K (2013) Pressure-responsive polymer membranes of slide-ring gels with movable cross-links. Adv Mater 25:4636–4640. https://doi.org/10.1002/adma.201301252

Khan AR, Forgo P, Stine KJ, D'Souza VT (1998) Methods for selective modifications of cyclodextrins. Chem Rev 98:1977–1996. https://doi.org/10.1021/cr970012b

Kidowaki M, Nakajima T, Araki J, Inomata A, Ishibashi H, Ito K (2007) Novel liquid crystalline polyrotaxane with movable mesogenic side chains. Macromolecules 40:6859–6862. https://doi.org/10.1021/ma070785u

Kim H, Kim YH, Lee S, Walba DM, Clark NA, Lee SB et al (2014) Orientation control over bent-core smectic liquid crystal phases. Liq Cryst 41:328–341. https://doi.org/10.1080/02678292.2013.817618

Koltzenburg S, Wolff D, Springer J, Nuyken O (1998) Novel study on the liquid crystalline behavior of poly (methacrylate) s with biphenyl side groups. J Polym Sci A Polym Chem 36:2669–2679. doi:10.1002/(SICI)1099-0518(19981115)36:15<2669::AID-POLA1>3.0.CO;2-4

Komiyama M, Hirai H (1983) Colloidal rhodium dispersions protected by cyclodextrins. Bull Chem Soc Jpn 56:2833–2834. https://doi.org/10.1246/bcsj.56.2833

Kumar S (2004) Recent developments in the chemistry of triphenylene-based discotic liquid crystals. Liq Cryst 31:1037–1059. https://doi.org/10.1080/02678290410001724746

Kumar S (2010) Chemistry of discotic liquid crystals: from monomers to polymers. CRC Press, Boca Raton

Kwak E-S, Gomez FA (1996) Determination of the binding of β-cyclodextrin derivatives to adamantane carboxylic acids using capillary electrophoresis. Chromatographia 43:659–662. https://doi.org/10.1007/BF02292984

Laschat S, Baro A, Steinke N, Giesselmann F, Hägele C, Scalia G et al (2007) Discotic liquid crystals: from tailor-made synthesis to plastic electronics. Angew Chem Int Ed 46:4832–4887. https://doi.org/10.1002/anie.200604203

Lee J, Jung K, Kim YS, Park D (2007) Diosgenin inhibits melanogenesis through the activation of phosphatidylinositol-3-kinase pathway (PI3K) signaling. Life Sci 81:249–254. https://doi.org/10.1016/j.lfs.2007.05.009

Lee E, Kim J-K, Lee M (2009) Reversible scrolling of two-dimensional sheets from the self-assembly of laterally grafted amphiphilic rods. Angew Chem Int Ed 48:3657–3660. https://doi.org/10.1002/anie.200900079

Liao Z, Du S, Qin Z, Wang J, Zuo F, Luo J (2015) Use of liquid crystals for imaging different inclusion abilities of α-cyclodextrin and β-cyclodextrin toward cetyltrimethyl ammonium bromide. Chem Phys Lett 637:189–194. https://doi.org/10.1016/j.cplett.2015.08.021

Lin H, Ding H, Kelly JR (1995) The mechanism of switching a PDLC film. Mol Cryst Liq Cryst 262:99–109. https://doi.org/10.1080/10587259508033516

Ling C-C, Darcy R, Risse W (1993) Cyclodextrin liquid crystals: synthesis and self-organisation of amphiphilic thio-β-cyclodextrins. J Chem Soc Chem Commun 438–440. doi:https://doi.org/10.1039/C39930000438.

Linlin D, Wei L, Jun C, Ban L, Shouxin L (2015) Formation, tuning and application of chiral nematic liquid crystal phase based on nanocrystalline cellulose. Prog Chem 27:861–869. https://doi.org/10.7536/PC141239

Liu Q-Y, Zuo F, Chong Y-Y, Zhao Z-G, Kwon Y, Chen J-X et al (2016) Molecular simulation of liquid crystal sensor based on competitive inclusion effect. J Incl Phenom Macrocycl Chem. https://doi.org/10.1007/s10847-016-0678-0

Lowe AM, Abbott NL (2012) Liquid crystalline materials for biological applications. Chem Mater 24:746–758. https://doi.org/10.1021/cm20263 2 m

Mamiya J, Kuriyama A, Yokota N, Yamada M, Ikeda T (2015) Photomobile polymer materials: photoresponsive behavior of cross-linked liquid-crystalline polymers with mesomorphic diarylethenes. Chem Eur J 21:3174–3177. https://doi.org/10.1002/chem.201406299

McArdle CB (1990) Side chain liquid crystal polymers. Springer Science & Business Media, New York

Mondal A, Jana NR (2012) Fluorescent detection of cholesterol using β-cyclodextrin functionalized graphene. Chem Commun 48:7316. https://doi.org/10.1039/c2cc33410k

Munir S, Park S-Y (2015) The development of a cholesterol biosensor using a liquid crystal/aqueous interface in a SDS-included β-cyclodextrin aqueous solution. Anal Chim Acta 893:101–107. https://doi.org/10.1016/j.aca.2015.08.051

Mushenheim PC, Trivedi RR, Weibel DB, Abbott NL (2014) Using liquid crystals to reveal how mechanical anisotropy changes interfacial behaviors of motile bacteria. Biophys J 107:255–265. https://doi.org/10.1016/j.bpj.2014.04.047

Nagarajan R (2002) Molecular packing parameter and surfactant self-assembly: the neglected role of the surfactant tail. Langmuir 18:31–38. https://doi.org/10.1021/la010831y

Noda Y, Hayashi Y, Ito K (2014) From topological gels to slide-ring materials. J Appl Polym Sci 131:n/a–n/a. https://doi.org/10.1002/app.40509

Oh CS (1977) Induced smectic mesomorphism by incompatible nematogens. Mol Cryst Liq Cryst 42:1–14. https://doi.org/10.1080/15421407708084491

Ohno K, Wong B, Haddleton DM (2001) Synthesis of well-defined cyclodextrin-core star polymers. J Polym Sci A Polym Chem 39:2206–2214. https://doi.org/10.1002/pola.1197.

Okawara M, Hashimoto F, Todo H, Sugibayashi K, Tokudome Y (2014) Effect of liquid crystals with cyclodextrin on the bioavailability of a poorly water-soluble compound, diosgenin, after its oral administration to rats. Int J Pharm 472:257–261. https://doi.org/10.1016/j.ijpharm.2014.06.032.

Okumura Y, Ito K (2001) The polyrotaxane gel: a topological gel by figure-of-eight cross-links. Adv Mater 13:485–487

Onuchak LA, Burmatnova TS, Spiryaeva EA, Kuraeva YG, Belousova ZP (2012) Sorption and selective properties of binary liquid-crystalline sorbent based on 4-Methoxy-4′-ethoxyazoxybenzene and a cetylated β-Cyclodextrin. Russ J Phys Chem A 86:1308–1317. https://doi.org/10.1134/S0036024412080080.

Oswald P, Pieranski P (2005) Smectic and columnar liquid crystals: concepts and physical properties illustrated by experiments. CRC Press. Available at: https://books.google.ca/books?hl=en&lr=&id=f4Q1m9cLEaEC&oi=fnd&pg=PP1&dq=Grandjean+terrace+mesophase+characteristics+of+smectic+liquid+crystals&ots=eRfiz3-CaM&sig=gd31p7B_9AcOzg3BokWm_7Vr-h0. Accessed 20 Feb 2017

Palepu R, Reinsborough VC (1990) β-cyclodextrin inclusion of adamantane derivatives in solution. Aust J Chem 43:2119–2123. https://doi.org/10.1071/ch9902119.

Paraschiv I, Tomkinson A, Giesbers M, Sudhölter EJ, Zuilhof H, Marcelis AT (2007) Amide, urea and thiourea-containing triphenylene derivatives: influence of H-bonding on mesomorphic properties. Liq Cryst 34:1029–1038. https://doi.org/10.1080/02678290701609640

Pari L, Monisha P, Mohamed Jalaludeen A (2012) Beneficial role of diosgenin on oxidative stress in aorta of streptozotocin induced diabetic rats. Eur J Pharmacol 691:143–150. https://doi.org/10.1016/j.ejphar.2012.06.038.

Park J-S, Abbott NL (2008) Ordering transitions in thermotropic liquid crystals induced by the interfacial assembly and enzymatic processing of oligopeptide amphiphiles. Adv Mater 20:1185–1190. https://doi.org/10.1002/adma.200702012.

Péchiné J-M, Meddour A, Courtieu J (2002) Monitoring the differential ordering of enantiomers included into cyclodextrins through deuterium NMR in lyotropic liquid crystals. Chem Commun:1734–1735. https://doi.org/10.1039/B205256C.

Petti L, Mormile P, Blau WJ (2003) Fast electro-optical switching and high contrast ratio in epoxy-based polymer dispersed liquid crystals. Opt Lasers Eng 39:369–377. https://doi.org/10.1016/S0143-8166(01)00119-1.

Prasad SK, Rao DS, Chandrasekhar S, Kumar S (2003) X-Ray studies on the columnar structures of discotic liquid crystals. Mol Cryst Liq Cryst 396:121–139. https://doi.org/10.1080/15421400390213258.

Rajewski RA, Stella VJ (1996) Pharmaceutical applications of cyclodextrins. 2. in vivo drug delivery. J Pharm Sci 85:1142–1169. https://doi.org/10.1021/js960075u.

Ram MK, Bertoncello P, Ding H, Paddeu S, Nicolini C (2001a) Cholesterol biosensors prepared by layer-by-layer technique. Biosens Bioelectron 16:849–856

Rani K, Garg P, Pundir CS (2004) Measurement of bile acid in serum and bile with arylamine-glass-bound 3α-hydroxysteroid dehydrogenase and diaphorase. Anal Biochem 332:32–37. https://doi.org/10.1016/j.ab.2004.02.039.

Rasheed A (2008) Cyclodextrins as drug carrier molecule: a review. Sci Pharm 76:567–598. https://doi.org/10.3797/scipharm.0808-05

Rosen MJ, Kunjappu DJT (2012) Surfactants and interfacial phenomena. Wiley, Hoboken

Saenger W, Müller-Fahrnow A (1988) Cyclodextrins increase surface tension and critical micelle concentrations of detergent solutions. Angew Chem Int Ed Eng 27:393–394. https://doi.org/10.1002/anie.198803931.

Saenger W, Noltemeyer M, Manor PC, Hingerty B, Klar B (1976) "Induced-fit"-type complex formation of the model enzyme α-cyclodextrin. Bioorg Chem 5:187–195. https://doi.org/10.1016/0045-2068(76)90007-9

Sergeyev S, Pisula W, Geerts YH (2007) Discotic liquid crystals: a new generation of organic semiconductors. Chem Soc Rev 36:1902–1929. https://doi.org/10.1039/B417320C

Serhatli IE, Kacar T (2006) Synthesis of liquid crystalline–amorphous block copolymers by combination of CFRP and ATRP mechanisms. J Appl Polym Sci 99:3187–3194. https://doi.org/10.1002/app.22036.

Shaikh VAE, Lonikar SV, Dhobale DA, Pawar GM (2007) Cholesterol-linked β-cyclodextrin—a thermotropic liquid-crystalline derivative. Bull Chem Soc Jpn 80:1975–1980. https://doi.org/10.1246/bcsj.80.1975

Shimizu T, Masuda M, Minamikawa H (2005) Supramolecular nanotube architectures based on amphiphilic molecules. Chem Rev 105:1401–1444. https://doi.org/10.1021/cr030072j.

Shiraishi Y, Toshima N, Maeda K, Yoshikawa H, Xu J, Kobayashi S (2002) Frequency modulation response of a liquid-crystal electro-optic device doped with nanoparticles. Appl Phys Lett 81:2845–2847. https://doi.org/10.1063/1.1511282

Shiraishi Y, Sugihara K, Okamura N, Sawai H, Kobayashi S, Toshima N (2012) Fast electro-optic switching of twisted nematic lcd doped with cyclodextrin capped silica nanoparticles. Macromol Symp 317–318:28–33. https://doi.org/10.1002/masy.201100066

Shiraishi Y, Tsujihata R, Sawai H, Kobayashi S, Toshima N (2015) Effect of particle size on electro-optic properties of liquid crystal devices doped with γ-cyclodextrin stabilized barium titanate nanoparticles. Mol Cryst Liq Cryst 611:100–108. https://doi.org/10.1080/15421406.2015.1028000.

Shiraishi Y, Watanabe C, Sawai H, Asano H, Toshima N (2016) Electro-optic function of liquid crystal displays doped with Poly(γ-cyclodextrin)-Protected ZrO_2 /Au nanoparticles. Macromol Symp 364:56–61. https://doi.org/10.1002/masy.201500150.

Song LX, Xu P (2008) A comparative study on the thermal decomposition behaviors between β-cyclodextrin and its inclusion complexes of organic amines. J Phys Chem A 112:11341–11348. https://doi.org/10.1021/jp806026q

Song LX, Teng CF, Xu P, Wang HM, Zhang ZQ, Liu QQ (2008) Thermal decomposition behaviors of β-cyclodextrin, its inclusion complexes of alkyl amines, and complexed β-cyclodextrin at different heating rates. J Incl Phenom Macrocycl Chem 60:223–233. https://doi.org/10.1007/s10847-007-9369-1

Stenzel-Rosenbaum MH, Davis TP, Chen V, Fane AG (2001) Synthesis of poly(styrene) star polymers grown from sucrose, glucose, and cyclodextrin cores via living radical polymerization mediated by a half-metallocene iron carbonyl complex. Macromolecules 34:5433–5438. https://doi.org/10.1021/ma0021803.

Suzuki M, Furue H, Kobayashi S (2001) Polarizerless nanomaterial doped guest-host LCD exhibiting high luminance and good legibility. Mol Cryst Liq Cryst Sci Technol Sect 368:191–196. https://doi.org/10.1080/10587250108029946.

Szejtli J, Huber O (2012) Proceedings of the fourth international symposium on cyclodextrins: Munich, West Germany, April 20–22, 1988. Springer Science & Business Media Available at: https://books.google.ca/books?hl=en&lr=&id=BCTpCAAAQBAJ&oi=fnd&pg=PA1&dq=Szejtli,+J.+ Cyclodextrin+Technology,+Kluwer+Academic+Publisher:+Dordrecht,+The+Netherlands,+1988.&ots = _snXLJcmEP&sig = BJZuOXtRoZ--QZPB2N3xKH30q2U. Accessed 13 Mar 2016

Takeo K, Ueraura K, Mitoh H (1988) Derivatives of α-cyclodextrin and the synthesis of 6-O-α-D-glucopyranosyl-α-cyclodextrin. J Carbohydr Chem 7:293–308. https://doi.org/10.1080/07328308808058926.

Tanaka MYI, Matsumoto M, Nakamura T, Yabe A, Nakanishi H, Kawabata Y (1987) Host–guest complexes of an amphiphilic β-cyclodextrin and azobenzene derivatives in Langmuir–Blodgett films. Kawabara H Takahashi Tamura W Tagaki H Nakahara K Fukuda. Chem Lett 1307. doi:https://doi.org/10.1246/cl.1987.1307.

Taneva S, Ariga K, Okahata Y, Tagaki W (1989) Association between amphiphilic cyclodextrins and cholesterol in mixed insoluble monolayers at the air-water interface. Langmuir 5:111–113. https://doi.org/10.1021/la00085a020.

Tolédano P, Neto AMF (1998) Phase transitions in complex fluids. World Scientific, Singapore

Uekama K (2004) Design and evaluation of cyclodextrin-based drug formulation. Chem Pharm Bull (Tokyo) 52:900–915. https://doi.org/10.1248/cpb.52.900

Ueno A, Breslow R (1982) Selective sulfonation of a secondary hydroxyl group of β-cyclodextrin. Tetrahedron Lett 23:3451–3454. https://doi.org/10.1016/S0040-4039(00)87639-X.

Valente AJM, Söderman O (2014) The formation of host–guest complexes between surfactants and cyclodextrins. Adv Colloid Interf Sci 205:156–176. https://doi.org/10.1016/j.cis.2013.08.001.

Verploegen E, Soulages J, Kozberg M, Zhang T, McKinley G, Hammond P (2009) Reversible switching of the shear modulus of photoresponsive liquid-crystalline polymers. Angew Chem Int Ed 48:3494–3498. https://doi.org/10.1002/anie.200900583.

Wan W, Monobe H, Tanaka Y, Shimizu Y (2003) Mesomorphic properties of copolyesters of 3, 6-linked triphenylene-based units and polymethylene spacers. Liq Cryst 30:571–578. https://doi.org/10.1080/0267829031000099608.

Wang S-J, Zhao R-Y, Yang S, Yu Z-Q, Chen E-Q (2014) A complex of poly (4-vinylpyridine) and tolane based hemi-phasmid benzoic acid: towards luminescent supramolecular side-chain liquid crystalline polymers. Chem Commun 50:8378–8381. https://doi.org/10.1039/C4CC03113J

Ward S, Calderon O, Zhang P, Sobchuk M, Keller SN, Williams VE et al (2014) Investigation into the role of the hydrogen bonding network in cyclodextrin-based self-assembling mesophases. J Mater Chem C 2:4928–4936. https://doi.org/10.1039/C4TC00448E

Wieckowski A, Savinova ER, Vayenas CG (2003) Catalysis and electrocatalysis at nanoparticle surfaces. CRC Press, New York

Yagai S, Kitamura A (2008) Recent advances in photoresponsive supramolecular self-assemblies. Chem Soc Rev 37:1520. https://doi.org/10.1039/b703092b.

Yallapu MM, Jaggi M, Chauhan SC (2010) Poly(β-cyclodextrin)/curcumin self-assembly: a novel approach to improve curcumin delivery and its therapeutic efficacy in prostate cancer cells. Macromol Biosci 10:1141–1151. https://doi.org/10.1002/mabi.201000084.

Yang F, Zhang Y, Guo H, Lin J (2013) Novel supramolecular liquid crystal: synthesis of cyclodextrin–triphenylene column liquid crystal based on click chemistry. Tetrahedron Lett 54:4953–4956. https://doi.org/10.1016/j.tetlet.2013.07.018.

Zhang P, Parrot-lopez H, Tchoreloff P, Baszkin A, Ling C, de Rango C et al (1992) Self-organizing systems based on amphiphilic cyclodextrin diesters. J Phys Org Chem 5:518–528. https://doi.org/10.1002/poc.610050814.

Zuo F, Liao Z, Zhao C, Qin Z, Li X, Zhang C et al (2014) An air-supported liquid crystal system for real-time reporting of host–guest inclusion events. Chem Commun 50:1857. https://doi.org/10.1039/c3cc48885c